Progress in Oceanography 165 (2018) 35–51

Contents lists available at ScienceDirect

Progress in Oceanography

journal homepage: www.elsevier.com/locate/pocean

Dissolved Organic Matter (DOM) in the open Mediterranean Sea. I. Basin–wide distribution and drivers of chromophoric DOM

Teresa S. Catalá[a,b,c,*], Alba María Martínez-Pérez[a], Mar Nieto-Cid[a], Marta Álvarez[d], Jaime Otero[a], Mikhail Emelianov[e], Isabel Reche[b], Javier Arístegui[f], Xosé Antón Álvarez-Salgado[a]

[a] CSIC Instituto de Investigacións Mariñas, Vigo, Spain
[b] Departamento de Ecología and Instituto del Agua, Universidad de Granada, Granada, Spain
[c] Research Group for Marine Geochemistry, Institute for Chemistry and Biology of the Marine Environment (ICBM), Carl von Ossietzky University Oldenburg, Oldenburg, Germany
[d] IEO Centro Oceanográfico de A Coruña, A Coruña, Spain
[e] CSIC Institut de Ciències del Mar, Barcelona, Spain
[f] Instituto de Oceanografía y Cambio Global (IOCAG), Universidad de Las Palmas de Gran Canaria, Las Palmas, Spain

ARTICLE INFO

Keywords:
Dissolved organic carbon
Chromophoric dissolved organic matter
Water masses
Biogeochemistry
Mediterranean Sea

ABSTRACT

Chromophoric dissolved organic matter (CDOM) in the open Mediterranean Sea (MedSea) is barely documented, remaining the basin–wide patterns in intermediate and deep waters still enigmatic. Here, full–depth distributions of CDOM absorption coefficients and spectral slopes recorded during the HOTMIX 2014 cruise are presented and their respective environmental drivers resolved. General Additive Models (GAMs) in surface waters and Optimum MultiParameter (OMP) water mass analysis in deep waters were applied. In the surface, apparent oxygen utilisation (AOU), a proxy to cumulative net community respiration, explained most of the variability of dissolved organic carbon (DOC) and the absorption coefficient at 254 nm (a_{254}), whereas the absorption coefficient at 325 nm (a_{325}), and the spectral slopes were mostly explained by potential temperature, a proxy to stratification and solar radiation, indicating that both water column stability and photobleaching may drive the variability of the UV–A absorbing CDOM components. In deep waters, the effect of water mass mixing and basin–scale mineralization were discerned from local mineralization processes. Water mass mixing and basin–scale mineralization contributed more substantially to explain the variability of DOC, a_{254} and a_{325} (82–91%) than the variability of the spectral slopes (35–64%). Local mineralization processes indicate that DOC and CDOM play a more relevant role in the carbon cycle in the Eastern (EastMed) than in the Western (WestMed) Mediterranean: whereas DOC contributed to 66 ± 10% of the oxygen demand in the EastMed, it represented only 24 ± 4% in the WestMed. Independently of basins and layers, a_{254} revealed as an excellent proxy to the concentration of DOC in the MedSea. Also, the unexpected inverse relationship of a_{325} with AOU indicates that the consumption of the UV–A absorbing CDOM fraction prevails over their production.

1. Introduction

The Mediterranean Sea, hereafter MedSea, represents 0.8% of the global ocean surface and is considered a laboratory basin for physical, chemical and biological ocean processes occurring on shorter temporal and spatial scales compared to the world ocean (Bergamasco and Malanotte-Rizzoli, 2010; The MerMex Group, 2011; Malanotte-Rizzoli et al., 2014). Geographically, it is made up of two semi–enclosed deep basins: western (WestMed) and eastern (EastMed). The thermohaline circulation of the MedSea is driven by the surface low salinity inflow of Atlantic Water (AW) at the Gibraltar Strait. As the AW moves eastwards, phytoplankton biomass and primary production decrease and the deep chlorophyll maximum (DCM) becomes deeper, reaching ultra oligotrophy in the EastMed (Azov, 1991; Yacobi et al., 1995; Moutin and Raimbault, 2002; Krom et al., 2010; Reygondeau et al., 2017). The bottom outflow at the Gibraltar Strait consists of a mixture of Levantine Intermediate Water (LIW), the saltiest water mass of the MedSea (Emelianov et al., 2017) with Eastern and Western Mediterranean Deep waters. The salinity maximum of the LIW is originated by convection in the south of Rhodes and can be traced throughout the entire MedSea between 200 and 500 m depth (Roether et al., 1998).

Deep waters of the MedSea are about 10 °C warmer than deep

* Corresponding author at: ICBM-MPI Bridging Group for Marine Geochemistry, Institute for Chemistry and Biology of the Marine Environment, Carl von Ossietzky University Oldenburg, Carl-von-Ossietzky-Straße 9-11, 26129 Oldenburg, Germany.
E-mail address: teresa.catala@uni-oldenburg.de (T.S. Catalá).

https://doi.org/10.1016/j.pocean.2018.05.002
Received 22 November 2017; Received in revised form 11 April 2018; Accepted 2 May 2018
Available online 07 May 2018
0079-6611/

Nomenclature

List of acronyms

a_{254}	absorption coefficient at 254 nm (in m^{-1})
a_{325}	absorption coefficient at 325 nm (in m^{-1})
AdDW	adriatic deep water
AdMW	middle adriatic water
AOU	apparent oxygen utilization (in $\mu mol\,kg^{-1}$)
AW	Atlantic Water
CDOM	chromophoric dissolved organic matter
CIW	Cretan Intermediate Water
DOC	dissolved organic carbon (in $\mu mol\,L^{-1}$)
DOM	dissolved organic matter
EastMed	Eastern Mediterranean Sea basin
EIW	Eastern Mediterranean Intermediate Water
EMDW	Eastern Mediterranean Deep Water
EMT	Eastern Mediterranean Transient
LIW	Levantine Intermediate Water
LSW	Levantine Surface Water
MAW	modified atlantic water
MedSea	Mediterranean Sea
NO	$O_2 + R_N \cdots CNO_3$ (in $\mu mol\,kg^{-1}$)
NO_3	nitrate concentration (in $\mu mol\,kg^{-1}$)
O_2	dissolved oxygen concentration (in $\mu mol\,kg^{-1}$)
PHA	prokaryotic heterotrophic abundance (in cell mL^{-1})
R_N	Redfield ratio, $-\Delta O_2/\Delta NO_3$ (in mol O_2 mol N^{-1})
S	salinity
$S_{275–295}$	spectral slope between 275 and 295 nm (in μm^{-1})
$S_{350–400}$	spectral slope between 350 and 400 nm (in μm^{-1})
SiO_4	silicate concentration (in $\mu mol\,kg^{-1}$)
S_R	ratio of the slope between 275 and 295 nm divided by the slope between 350 and 400 nm
WestMed	Western Mediterranean Sea basin
WIW	Winter Intermediate Water
WMDW	Western Mediterranean Deep Water
WMT	Western Mediterranean Transition
Z	depth (in m)
θ	potential temperature (in °C)

waters of the global ocean; they form every winter in both the WestMed and EastMed by a mechanism analogous to the polar Atlantic deep convection. The Eastern Mediterranean Deep Water (EMDW) is formed in the Ionian Sea, when water from the Southern Adriatic Sea plunges down through the Otranto Strait and sinks to depths > 3000 m. Then, it flows eastwards and occupies the water column below the LIW with a temperature > 13.3 °C and salinity > 38.66 (Wu et al., 2000). In the 1990s, for a short period of time, during the so–called Eastern Mediterranean Transient (EMT), the formation site of deep water changed from the Adriatic to the Aegean Sea. The cause was an abrupt climate shift in this area, which resulted in a warmer, more saline and denser deep water mass than the previously existing EMDW of Adriatic origin (Roether et al., 1996; Lascaratos et al., 1999; Klein et al., 2003). After the EMT, EMDW started to form again in the Ionian Sea. Therefore, the EMT altered the formation and large–scale circulation of the EastMed deep waters (Roether et al., 1996, 2007), which is imprinted in the pre–EMT, EMT and post–EMT EMDW varieties currently found in the deep EastMed. The WDMW is formed in winter in the Gulf of Lions (Gascard, 1978) and occupies the water column below the LIW with temperatures between 12.75 and 12.80 °C and salinities between 38.44 and 38.46 (Millot, 1999). During the winter of 2004–05, a strong convention event in the Gulf of Lions (called Western Mediterranean Transition) led to the formation of a new WMDW variety, saltier and slightly warmer than previously (salinity of 38.47–38.50 and temperature of 12.87–12.90 °C; López-Jurado et al., 2005; Beuvier et al., 2012; Schroeder et al., 2016). Therefore, like in the EastMed, different varieties of the WMDW coexist in the bathypelagic layer of the WestMed.

In the epipelagic MedSea, an increase in the concentration of dissolved organic carbon (DOC) from West to East has been observed (Santinelli et al., 2012, 2013) in parallel to the rising oligotrophy of the AW flowing eastwards (Moutin and Raimbault, 2002; Reygondeau et al., 2017). This accumulation of DOC is characteristic of oligotrophic areas since nutrients shortage limits the microbial degradation of dissolved organic matter (DOM) (Thingstad et al., 1997; Hansell et al., 2009; Romera-Castillo et al., 2016). The distribution of DOC in the meso– and bathypelagic MedSea is also well–known (Santinelli et al., 2010, 2012; Santinelli, 2015). DOC concentrations in the EMDW and WMDW are at the level of the lowest values reported for the deep Atlantic and Pacific oceans (36–42 $\mu mol\,L^{-1}$; Santinelli, 2015 and literature therein). This is unexpected given the short renewal time of the MedSea (20–126 years; Andrie and Merlivat, 1988; Schlitzer et al., 1991) and the noticeable inputs of terrestrial carbon from Europe and North Africa (Mladenov et al., 2011; Santinelli, 2015). It is remarkable the large contribution of DOC to the oxygen demand of the LIW (30–50%; Santinelli et al., 2010, 2012; Martínez-Pérez et al., 2017a) as compared with the open world ocean (10–20%; Arístegui et al., 2002). Furthermore, in the deep MedSea, the DOC mineralization rates are estimated in 1.4–14.4 $\mu M\,C\,yr^{-1}$ (Santinelli et al., 2010; Hansell et al., 2012; Martínez-Pérez et al., 2017a), which are substantially higher than the largest values reported for the open ocean (0.1–0.9 $\mu M\,C\,yr^{-1}$; Carlson et al., 2010). In this regard, carbon isotopic data ($\Delta^{14}C$ and $\delta^{13}C$) support the idea that up to 45% of the refractory DOC transported by the AW is removed in the deep MedSea in less than 126 yr (Santinelli et al., 2015). In terms of molecular composition, Martínez-Pérez et al. (2017b) have recently characterized the DOM of the MedSea and the adjacent Northeast Atlantic Ocean by Fourier Transform Ion Cyclotron Resonance Mass Spectrometry (FT–ICR–MS). Their results showed a more reworked DOM in the Mediterranean overflow water than in the Atlantic Inflow. Moreover, as the water masses of the MedSea aged, lower DOC concentrations but higher average molecular weight and highly unsaturated compounds were found. The contrasting origin, Aegean or Adriatic, of the EMDW, also affect the molecular composition of DOM.

Contrary to DOC, the dynamics of the chromophoric fraction of DOM (CDOM), i.e. the organic compounds that absorbs light in the UV and visible ranges of the light spectrum, is barely documented in the MedSea. Although CDOM is a small fraction of the total DOM pool in the open ocean (Nelson et al., 1998, 2010; Nelson and Siegel, 2002; Siegel et al., 2002), it plays an important role in the carbon cycle (Mopper and Kieber, 2002) and in the optical properties of seawater (Organelli et al., 2014; Sempéré et al., 2015). It can contribute more than 50% to the light absorption at 440 nm at the ocean surface (Bricaud et al., 2002, 2010; Siegel et al., 2002; Babin et al., 2003) and its contribution can increase up to almost 100% below the deep chlorophyll maximum (Bricaud et al., 2010). In the MedSea, CDOM values from the upper layers have been reported only very recently (Organelli et al., 2014; Xing et al., 2012, 2014; Pérez et al., 2016; Pitta et al., 2016). However, basin–wide patterns of CDOM in the intermediate and deep Mediterranean waters are currently unknown, likely due to technical constrains of the standard spectrophotometric procedures.

In this context, the aim of this study is to disclose the full–depth distributions of CDOM across the open MedSea and to determine the physical and biogeochemical drivers responsible for those distributions. Particularly, we expect that CDOM in the MedSea behaves different

than in the World Ocean and that the increasing oligotrophy from the WestMed to the EastMed produce a contrasting response of CDOM parameters in the two MedSea basins. Since the hydrographic properties are not conservative in the surface layer because of mass and heat exchange with the atmosphere, we used General Additive Models (GAMs) to resolve the key environmental drivers of CDOM variability in the epipelagic layer. On the contrary, the conservativeness of the hydrographic properties in the meso– and bathypelagic layers allowed us to use an Optimum MultiParameter (OMP) water mass analysis to differentiate the impact of water mass mixing and basin scale mineralization from the local biogeochemical processes on the distributions of CDOM.

2. Materials and methods

2.1. General sampling strategy and analytical methods

During the HOTMIX 2014 cruise, on board the R/V Sarmiento de Gamboa (Heraklion, Crete, 27 April 2014 – Las Palmas, Canary Islands, 29 May 2014), 24 hydrographic stations were occupied along the whole Mediterranean Sea (Fig. 1).

A total of 330 discrete water samples (max. 15 levels per station) were collected using a SBE38 rosette sampler equipped with 24 (12 L) Niskin bottles. Two conductivity, temperature and depth probes (CTD SBE 911 plus) were attached to the rosette, along with dissolved oxygen (SBE–43 oxygen sensor) and fluorescence of chlorophyll *a* (SeaPoint fluorometer) sensors. Discrete sampling depths were selected inspecting real time profiles of potential temperature, salinity, dissolved oxygen and fluorescence. In all stations, the deepest sample was collected near the seafloor.

The salinity, dissolved oxygen (O_2) and fluorescence of chlorophyll *a* (Chl *a*) sensors were calibrated with discrete samples measured on board.

2.1.1. Determination of the explanatory variables: salinity, inorganic nutrients, O_2, Chl a and bacterial biomass

Samples for salinity were measured with a Guideline Portasal salinometer Model 8410A. Conductivity measurements were converted into practical salinity scale values (UNESCO, 1985). Samples for O_2 determination were collected in flared neck iodine calibrated flasks and measured using a Winkler potentiometric method adapted from Langdon (2010). The apparent oxygen utilization was calculated as $AOU = O_2sat - O_2$ (Benson & Krause, UNESCO, 1986), where O_2sat is the oxygen saturation. Chl *a* measurements were performed by filtering 500 mL of water through a Whatman GF/F filter and stored frozen until analysis on board. Chl *a* pigments were extracted in cold acetone (90% v/v) for 24 h and analysed with a 10 AU Turner Designs bench fluorometer, previously calibrated with pure Chl *a* (Sigma Aldrich) (Holm-Hansen et al., 1965). Samples for inorganic nutrient analysis were collected in 50 mL polyethylene bottles and kept in the dark at 4 °C until analysis on board. Nitrate, phosphate and silicate concentrations were determined using a Skalar segmented flow autoanalyzer SAN++ following the colorimetric methods of Grasshoff et al. (1999).

The heterotrophic prokaryote abundance (PHA) was estimated by flow cytometry. Samples (1.6 mL) were preserved with paraformaldehyde (2% final concentration), left 15 min at 4 °C in the dark to fix, deep frozen in liquid nitrogen and stored at −80 °C until analysed. The day after, subsamples (400 µL) were stained with the fluorochrome SYBR Green I, Molecular Probes (final concentration 1000x dilution of the commercial product) at room temperature before analyses at low speed ($< 20\ \mu L\ min^{-1}$) with a BD FACSCalibur cytometer, fitted with a 15 mW laser emitting at 488 nm. Cells were identified in bivariate plots of side scatter (SSC–H) versus green fluorescence (FL1–H). A suspension of yellow–green 1 µm latex beads ($\sim 10^6$ beads mL^{-1}) was added as an internal standard (Polysciences, Inc.).

2.1.2. Determination of the response variables: DOC and CDOM

Seawater samples for the determination of DOC and CDOM were collected in 0.25 L acid–cleaned glass bottles and stored in the dark. Surface samples (< 200 m) were filtered through precombusted (450 °C, 4 h) Whatman GF/F filters with an acid–cleaned all–glass filtration system under positive pressure of high–purity N_2, previously rinsed with about 50 mL of the sample. Absorption of DOC onto GF/F filters in open ocean samples, estimated as the amount of carbon retained on a backing filter placed underneath the main filter, used to be $< 0.5\ \mu mol\ C\ L^{-1}$ (e.g. Santana-Falcón et al., 2017). Therefore, a significant effect of CDOM adsorption onto GF/F is not expected. Deep ocean samples (> 200 m) were not filtered because light absorption due to pigments and detrital particles contribute only to a minor fraction of the deep open ocean CDOM absorption (Nelson et al., 1998, 2007).

Aliquots of 10 mL were collected for DOC determination in precombusted (450 °C, 12 h) glass ampoules. These samples were acidified to pH < 2 and the ampoules were heat–sealed and stored in the dark at 4 °C until analysis in the base laboratory. DOC concentration was determined with a Shimadzu TOC–V organic carbon analyser by high temperature catalytic oxidation. Potassium hydrogen phthalate (99.95–100.05%, p.a., Merck) was used to calibrate the system daily. The precision of the equipment was $\pm\ 1\ \mu mol\ L^{-1}$. The accuracy was checked daily with the DOC reference materials provided by D. A. Hansell (University of Miami, USA). All DOC samples were measured within 6 months.

The UV–Visible–NIR absorption spectra of CDOM were measured on board from 178 nm to 879 nm at 0.38 nm intervals by using a 100 cm path length liquid waveguide capillary cell (LWCC) from World Precision Instruments (model LPC100CM), a Deuterium–Halogen Light Sources for the UV–Vis (Ocean Optics model DH2000BAC) and a miniature spectrometer (Ocean Optics model USB2000 + UV–VIS). Finally,

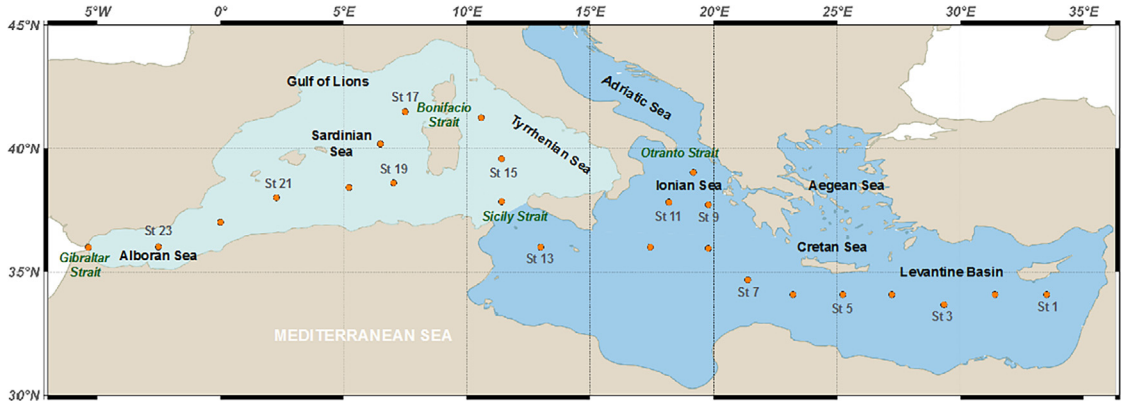

Fig. 1. Sampling stations during the Hotmix cruise.

two 600 µm fibber optic cables (Ocean Optics model QP600–1–SR–BX) connected the LWCC with the light source and the spectrometer. The LWCC is made of quartz capillary tubing coated with a low refractive index polymer. Therefore, these cells are designed to minimize absorbance biases due to changes in the refractive index between samples of different salinity and the waveguide. In the particular case of our LWCC, 10% and 50% dilutions of filtered (0.2 µm) natural seawater of salinity 35.9 yielded average differences of $0.005 \pm 0.005\ m^{-1}$ at any wavelength between the measured and the expected concentration according to the sample dilution. This result prevented us to make any further correction of the refractive index in our measurements. Prior to measuring, the reference (Milli–Q water) and the samples were acclimatized at room temperature to minimize temperature effects. Each sample was measured twice and the average of the two spectra was reported. Only the absorbances (Abs) from 250 nm and 700 nm were logged. A baseline correction was applied by subtracting the average absorbance between 600 and 700 nm to the measured absorption spectrum. Finally, corrected absorbances were converted into naeperian absorption coefficients (a_λ) multiplying by 2.303 and dividing by the light pathlength, which was of 99.89 cm as certified by World Precision Instruments.

In this study, we will focus on the absorption coefficients at wavelengths 254 nm, a_{254}, and 325 nm, a_{325}, and the spectral slopes for the wavelength bands 275–295 nm, $S_{275–295}$, and 350–400 nm, and $S_{350–400}$ (Helms et al., 2008). These spectral slopes were calculated from the linear regression of the log–transformed absorption spectra. Only those $S_{275–295}$ with $R^2 > 0.95$ and those $S_{350–400}$ with $R^2 > 0.80$ were retained. Finally, the slope ratio (S_R) was calculated as the ratio of the slope of the shorter wavelength band (275–295 nm) to that of the longer wavelength band (350–400 nm). Given that in the open MedSea nitrate concentrations are $< 10\ \mu mol\ kg^{-1}$, the effect on nitrate absorption on a_{325} and spectral slopes is minor and was not corrected (Catalá et al., 2016). a_{254} is proportional to the abundance of conjugated carbon double bonds and it has been suggested as a proxy for the concentration of DOC (e.g. Lønborg and Álvarez-Salgado, 2014), whereas a_{325} is an indicator of the presence of aromatic substances (Nelson et al., 2004; Catalá et al., 2015). The slopes of the 275–295 nm region and S_R have been related to DOM molecular weight and to its corresponding photochemically induced shifts (Helms et al., 2008).

2.2. Generalized additive models (GAMs)

To assess the effect of the environmental conditions on the basin-wide variability of DOC and CDOM in the epipelagic layer of the

Table 1a
Main water masses in the Eastern Mediterranean Sea with a brief description of their characteristics and some references where more information about their origin and circulation can be found. The Water Types (WT) used to model them are shown.

Name	Source	Characteristics	Acronym & WT	References
Modified Atlantic water	Atlantic Ocean	MAW derives from the Atlantic Water entering the MedSea at the Strait of Gibraltar, in the way to the Strait of Sicily it mixes, evaporates and loses nutrients. MAW enters the EMED crossing the Strait of Sicily in the surface layer following a cyclonic path. Here is identified by a minimum of salinity	MAW	Manzella and La Violette (1990) Millot (1999) Lermusiaux and Robinson (2001)
Levantine Surface Water	Levantine Basin	Highly modified Atlantic Water, detected by a surface maximum of salinity ($S > 39$) and temperature ($> 17\ ^\circ C$)	LSW	Theocharis et al. (1993) Özturgut (1976)
Levantine Intermediate Water	Rhodes Gyre ($\sim 30^\circ E$)	Formed by the combined effects of evaporation, increasing salinity in summer, and relatively deep vertical mixing caused by intense dry northerly winds in winter. It flows at mid depths (200–500 m) in the EMED. Typically presents $S = 38.74–39.20$ and $\theta = 15–17\ ^\circ C$ in the Levantine Basin	LIW	Özturgut (1976) Wüst (1961) Millot (2013) Lascaratos et al. (1993)
Cretan Intermediate Water	Cretan Sea	Outflowing water from the Cretan Sea into the EastMed through the Cretan Arc straits. It is colder, less saline and denser than LIW, so it is found between LIW and EMDW. It moves westward along the Cretan continental slope towards the Ionian and Adriatic seas	CIW	Astraldi et al. (1999) Theocharis et al. (1999) Velaoras et al. (2014) Schlitzer et al. (1991)
Middle Adriatic Water	Adriatic Sea	Operative water type defined from data in the Adriatic Pit taken from the M84/3 cruise in 2011. This WT is influenced by Adriatic Surface Water with a low salinity and temperature, around 400 dbar, and detected in the eastern Ionian Sea	AdMW	Velaoras et al. (2014) Vilibić and Orlić (2002)
Adriatic Deep Water	Adriatic Sea	Formed in the Southern Adriatic Pit where a cyclonic gyre is nearly permanently present, produced by open ocean deep convection from water preconditioned by LIW and CIW. This water spills over the Ionian Sea following the western part	AdDW	Artegiani et al. (1993) Rubino and Hainbucher (2007)
Eastern Mediterranean Deep Water (EMDW)	Adriatic Sea	The Adriatic Sea was the source of deep waters to the EastMed prior to the EMT event (1987–1995). This water is less saline, warmer and denser than EMDW produced during the post–EMT phase	Pre–EMT	Roether et al. (1996) Lascaratos et al. (1999)
	Aegean Sea	EMDW produced in the Cretan / Aegean Sea during the EMT event (1995–1999). This denser water compared to Pre–EMT caused an uplifting of the bottom isopycnals. The EMDW with Aegean Sea origin produced during the EMT event is warmer, more saline and less oxygenated than the Pre-EMT water of Adriatic origin	EMT	Roether et al. (1996) Roether et al. (2007) Lascaratos et al. (1999) Klein et al. (1999)
	Adriatic Sea	After the EMT event, the Adriatic Sea started to produce again EastMed. This Post–EMT EMDW is mainly found in the Levantine basin from 2007s. This water is colder and less saline than the EMT water type	Post–EMT–A	Manca et al. (2003) Sparnocchia et al. (2011) Kovačević et al. (2012)
	Adriatic Sea	After 2003s Adriatic Deep Water became warmer and saltier than that previously produced. This water is still found in the Ionian basin in 2011	Post–EMT–B	Rubino and Hainbucher (2007) Hainbucher et al. (2006) Cardin et al. (2015)
	Adriatic Sea	After 2007 s Adriatic Deep Water spilling is still getting saltier and warmer and found over the bottom of the Ionian Sea. This newer deep water is also detected by a higher oxygen	Post–EMT–C	Rubino and Hainbucher (2007) Hainbucher et al. (2006) Bensi et al. (2013)

MedSea we used generalized additive models (GAMs, Wood, 2006). We examined the influence of the environmental explanatory variables described above on the response variables DOC, a_{254}, a_{325}, $S_{275–295}$ and S_R. Before model fitting, covariability among predictors was examined using variance inflation factors (VIFs, Table S1). GAMs were formulated as follows:

$$Y_{i,l} = \alpha + \sum_j g_j(X^j{}_{i,l}) + \in_{i,l} \quad (1)$$

where Y is DOC, a_{254}, a_{325}, $S_{275–295}$ or S_R measured at a station i and depth level l, α is an intercept, X is a vector of predictor variables where the superscript j identifies each covariate, g is a non–parametric smoothing function specifying the effect of each covariates on the response variables and $\in_{i,l}$ is the error term assumed to be normally distributed. Smoothing functions were fit by penalized cubic regression splines restricted to a maximum of three knots. The smoothness of the functions was estimated by minimizing the generalized cross validation criterion. Results from the GAM analysis of DOC and CDOM variables are summarised in Tables S2 and S3, respectively. All models were fitted in R 3.2.3 software (R Development Core Team, 2014) and using the 'mgcv 1.8–16' package (Wood, 2006).

2.3. Optimum MultiParameter (OMP) water mass analysis

The cornerstone of an OMP water mass analysis is the identification and quantification of the water types that contribute to the water samples collected in a certain study area. In this regard, a water type (WT) is a unique combination of potential temperature, salinity and other tracer values used to unambiguously define a given water mass (Tomczak, 1999). Particularly, the variables used to define the water types in our OMP analysis are potential temperature (θ), salinity (S), the conservative chemical parameter NO ($NO = O_2 + R_N * NO_3$, Broecker, 1974) and silicate (SiO_4). R_N is the stoichiometric ratio of dissolved oxygen consumption to nitrate production during the mineralization of biogenic organic matter in the ocean, which has been fixed at 9.3 mol O_2 mol ${NO_3}^{-1}$ (Anderson, 1995).

Despite having a relatively small area, the MedSea contains a wide variety of surface, intermediate and deep water masses (e.g., Schroeder et al., 2012), which makes setting and solving an OMP analysis particularly difficult. A detailed description of our OMP analysis can be found in Section 2 of the supplementary material. In brief, the oceanographic setting found during the HOTMIX 2014 cruise can be effectively explained with the array of water types described in Table 1. Note that the Eastern (Table 1a) and Western (Table 1b) basins are considered separately. The physical properties of these water types (Table 2) were extracted from the literature and corresponded to the θ and S of the water types in their formation area or when they enter a given MedSea basin. The θ–S pairs of the water types should envelope the θ–S diagrams of the CTD profiles collected during the cruise, as shown in Figs. S1 and S2.

The chemical properties of each water type were estimated from a linear regression analysis of NO and SiO_4 with S or θ within the realm of that water type (Álvarez et al., 2014). Following Poole and Tomczak (1999), the standard error of these regression equations have been used to compute the uncertainty of the estimation of the water type characteristics (Table 2). Samples collected in the upper layer cannot be included in the OMP analysis because θ, S and NO do not behave conservatively due to the air–sea exchange of heat, water and gases and SiO_4 is affected by biological utilization.

The mass balance equations involved in our OMP analysis are:

$$\begin{aligned} &\sum_i x_{ij} \cdot \theta_i = \theta_j + \mathrm{R}\theta\mathrm{j} \\ &\sum_i x_{ij} \cdot S_i = S_j + \mathrm{RSj} \\ &\sum_i x_{ij} \cdot NO_i = NO_j + \mathrm{RNOj} \\ &\sum_i x_{ij} \cdot (SiO_4)_i = (SiO_4)_j + \mathrm{RSiO4j} \\ &\sum_i x_{ij} = 1 + \mathrm{R} \sum \end{aligned} \quad (2)$$

where x_{ij} is the proportion of water type i in sample j; θ_i, S_i, NO_i and SiO_{4i} are the values of θ, S, NO and SiO_4 of water type i shown in

Table 1b
Main water masses in the Western Mediterranean Sea with a brief description of their characteristics and some references where more information about their origin and circulation can be found. The Water Types (WT) used to model them are shown.

Name	Source	Characteristics	Acronym & WT	References
Atlantic Water (AW)	Atlantic Ocean	Surface Atlantic Water entering the MedSea at the Strait of Gibraltar flows anticlockwise suffering continuous modifications by mixing and evaporation. It is identified by a minimum in salinity in the upper surface layer and it contains very low nutrients	AW	Millot (1999) Huertas et al. (2012)
Eastern Intermediate Water	Strait of Sicily	Recently named by Millot (2013). High salinity intermediate waters from the EastMed (i.e. LIW and CIW) flow into the WestMed also mixing with transitional EMDW. Recognized in the WestMed by its maximum in temperature and salinity, contains relatively more nutrients than LIW	EIW	Millot (2013) Astraldi et al. (1999) Gasparini et al. (2005) Astraldi et al. (2002)
Western Intermediate Water	NW basin	The WIW is formed in the continental shelf of the Gulf of Lion and the Balearic Sea through severe winter convection. Recognized by relative minimum in temperature between the surface AW and WMDW	WIW	Millot (1999) Salat and Font (1987) Sparnocchia et al. (1999)
Western Mediterranean Deep Water (WMDW)	NW basin	The oldest resident WMDW water in the WestMed formed prior to the WMT (before 2004/5) by deep convection in the Gulf of Lion. Nowadays detected as a deep relative minimum in temperature and salinity. We use the nomenclature in (11) to name the different vintages of WMDW	A	Bethoux and Tailliez (1994) MEDOC Group (1970) Schroeder et al. (2006)
	NW basin	Originated during the extreme forcing conditions in winter 2004/5 by open sea convection, mainly in the Gulf of Lions, as preconditioned with saltier and warmer CIW and LIW, this WMDW is warmer and saltier than the previous resident one, A	B	Schroeder et al. (2006) López-Jurado et al. (2005)
	NW basin	Originated during the extreme forcing conditions in winter 2004/5 but with a higher influence of coastal shelf waters, it is fresher, colder and more oxygenated than B	C	Schroeder et al. (2006) Puig et al. (2013)
	NW basin	Each winter since 2009/10, but especially in 2011/12, warmer, saltier and denser deep water is produced, uplifting the older deep waters near the bottom, we operationally call the more recent WestMed types found in 2011 and 2014 as D11 and D14, clearly distinguished in the temperature-salinity diagrams	D	Puig et al. (2013) Schroeder et al. (2016) Houpert et al. (2016)

Table 2
Thermohaline and chemical characteristics (average value ± uncertainty) of the water types defined to model the mixing of Mediterranean water masses along the HOTMIX cruise, separating Eastern and Western basins. R^2 determination coefficient; and SE, standard error of the residuals from the regression between measured and back–calculated variables; and N, number of data. Only data for the meso- and bathypelagic layers are considered.

Acronym	θ_i(°C)	S_i	SiO_{4i} (μmol kg^{-1})	NO_i(μmol kg^{-1})
Eastern Mediterranean Basin				
MAW	14.740 ± 0.002	37.150 ± 0.005	0.6 ± 0.3	250 ± 5
LSW	17.800 ± 0.002	39.180 ± 0.005	0.7 ± 0.3	221 ± 5
LIW	16.910 ± 0.002	39.270 ± 0.005	0.9 ± 0.3	219 ± 5
CIW	15.000 ± 0.002	39.140 ± 0.005	4.0 ± 0.3	234 ± 5
AdMW	13.790 ± 0.002	38.732 ± 0.005	1.1 ± 0.3	250 ± 5
AdDW	13.520 ± 0.002	38.705 ± 0.005	3.1 ± 0.3	250 ± 5
Pre–EMT	13.570 ± 0.002	38.744 ± 0.005	9.1 ± 0.3	228 ± 5
EMT	13.640 ± 0.002	38.788 ± 0.005	7.8 ± 0.3	229 ± 5
Post–EMT–A	13.500 ± 0.002	38.756 ± 0.005	7.2 ± 0.3	237 ± 5
Post–EMT–B	13.400 ± 0.002	38.717 ± 0.005	6.3 ± 0.3	240 ± 5
Post–EMT–C	13.420 ± 0.002	38.735 ± 0.005	6.3 ± 0.3	238 ± 5
R^2	0.9984	0.9989	0.9987	0.72
SE	0.014	0.005	0.10	2.7
N	100	100	100	100
Western Mediterranean Basin				
AW	14.800 ± 0.002	37.000 ± 0.005	0.9 ± 0.3	254 ± 5
EIW	14.220 ± 0.002	38.840 ± 0.005	5.9 ± 0.3	226 ± 5
WIW	12.934 ± 0.002	38.259 ± 0.005	1.6 ± 0.3	262 ± 5
A	12.840 ± 0.002	38.460 ± 0.005	9.3 ± 0.3	268 ± 5
B	12.910 ± 0.002	38.480 ± 0.005	7.8 ± 0.3	271 ± 5
C	12.881 ± 0.002	38.477 ± 0.005	8.4 ± 0.3	275 ± 5
D11	12.902 ± 0.002	38.486 ± 0.005	7.7 ± 0.3	280 ± 5
D14	12.913 ± 0.002	38.492 ± 0.005	9.5 ± 0.3	283 ± 5
R^2	0.9987	0.9967	0.9859	0.95
SE	0.013	0.005	0.21	3.2
N	75	75	75	75

Table 2; θ_j, S_j, NO_j and SiO_{4j} are the values of θ, S, NO and SiO_4 in sample j; and $R\theta_j$, RS_j, RNO_j, $RSiO_{4j}$ and RΣ are the residuals of the mass balance equations of θ, S, NO, SiO_4 and mass conservation for sample j. A restriction to this system of equations is that the values of x_{ij} have to be ≥0% (a negative proportion has no physical sense). The linear mixing equations are normalized and weighted. The normalization is done using the mean and standard deviation values of the four parameters in Table 2. Equations are weighted taking into account the measurement error of each parameter in relation with its variability in the study area and its relative conservative nature. Weights of 8, 8, 1 and 2 were assigned to θ, S, NO and SiO_4, respectively. As the stoichiometry ratio R_N of NO is variable and SiO_4 is influenced by silica dissolution, we assigned lower weights to their respective mass balance equations. The mass conservation equation is stringently resolved by assigning a weight of 100 to it.

In order to solve the OMP it is crucial to define mixing groups, this is, which water masses mix and in which basin, maintaining the horizontal and vertical connection or continuity between basins. The groups defined in our OMP are explained in the supplementary material and summarised in Table S4.

As discussed in Álvarez et al. (2014), the reliability of the OMP analysis can be informed by checking the determination coefficient (R^2) and the standard error of the estimation (SE) of the linear regression between the measured and back–calculated values for the input variables, S, θ, NO and SiO_4 and the distribution of the total and individual residuals from the system of mass balance Eq. (2). The back–calculated fields are obtained multiplying the OMP water mass proportions (x_{ij}) by the water type values of S, θ, NO and SiO_4. Note that R^2 was high and SE was slightly above that of the measurement error for any of the input variables in both the EastMed and the WestMed (Table 2). Furthermore, the vertical distributions of the total and individual residuals of the mass balance equations are shown in Fig. S3. They are very low below 200 m depth. Further details about the OMP settings, reliability and results can be found in the supplementary material.

2.4. Assessing the impact of water mass mixing and biogeochemistry in the distribution of the explanatory and response variables

2.4.1. Water mass mixing weighted–average values

The water mass mixing weighted–average value, hereinafter archetype value, of any variable (N) in a given water mass can be obtained as:

$$\langle N_i \rangle = \frac{\sum_j x_{ij} \cdot N_j}{\sum_j x_{ij}} \quad (3)$$

where $\langle N_i \rangle$ is the archetype value of N in water mass *i*; N_j is the value of N in sample j; and x_{ij} is the proportion of water mass *i* in sample j. The standard deviation (SD) of the archetype value of N is calculated as:

$$SDN_i = \frac{\sqrt{\sum_j x_{ij} \cdot (N_j - \langle N_i \rangle)^2}}{\sum_j x_{ij}} \quad (4)$$

Application of Eq. (3) to the longitude, latitude and depth of the samples allowed the calculation of the centre of mass or barycentre of each water mass.

Finally, the proportion of the total volume of the samples occupied by a given water mass (%VOL_i) was calculated as:

$$\langle \%VOL_i \rangle = 100 \cdot \frac{\sum_j x_{ij}}{n} \quad (5)$$

where n = 244, is the number of samples included in the OMP analysis.

2.4.2. Mixing model of DOC and CDOM

The fraction of the total variability of parameter N due to water mass mixing can be calculated from the multiple linear regression of N_j with the previously obtained x_{ij} values. A system of n linear equations (one per sample) with m coefficients (one per WT) has to be solved for each chemical variable:

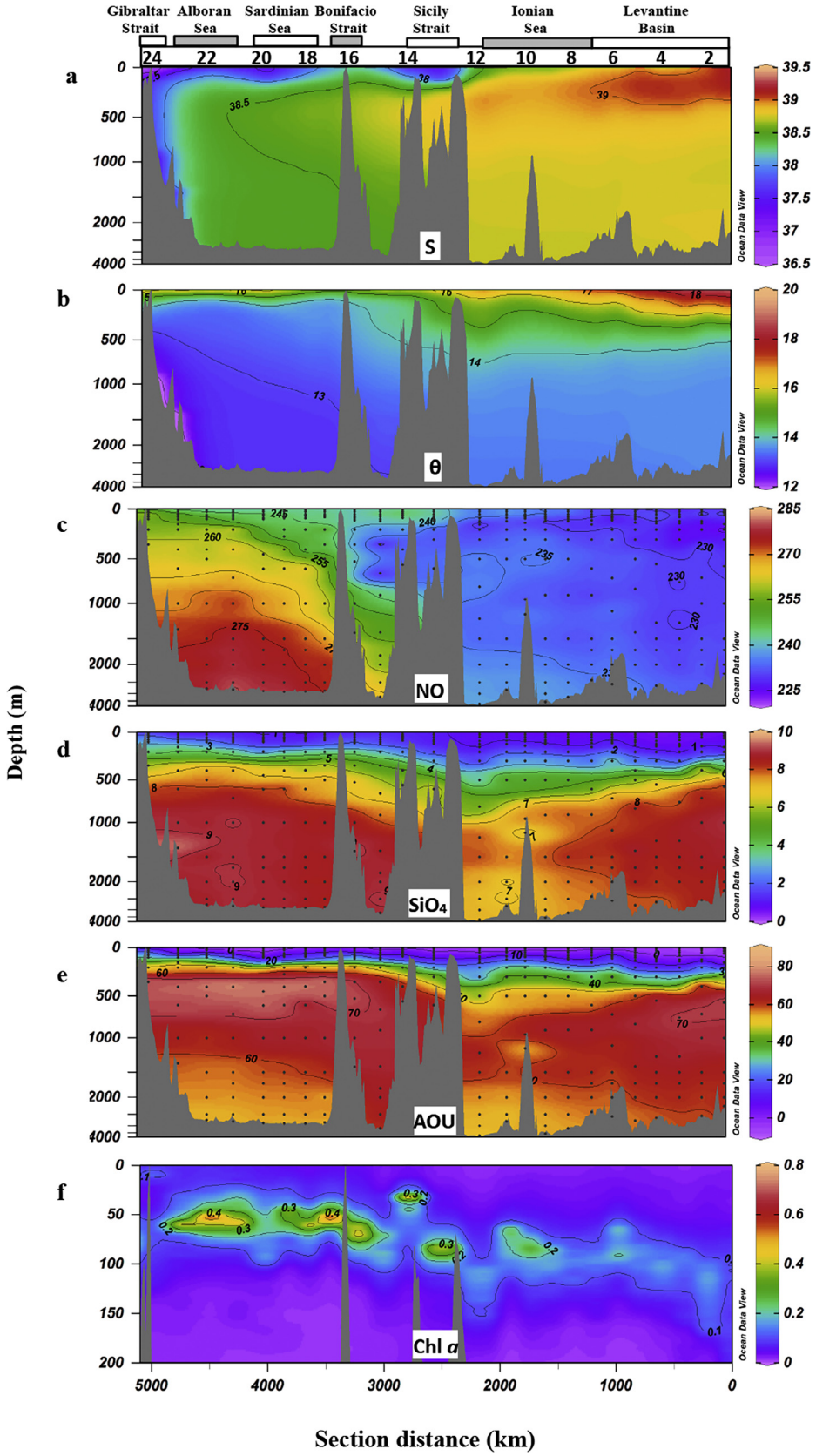

Fig. 2. Distribution of the variables used to run the OMP analysis: (a) salinity (S), (b) potential temperature (θ, °C), (c) NO (μmol kg^{-1}), (d) silicate (SiO_4, μmol kg^{-1}). Besides (e) apparent oxygen utilization (AOU, μmol kg^{-1}) and (f) fluorescence of chlorophyll *a* (Chl *a*, fluorescence units) are represented. Note that the depth of Chl *a* is displayed for the upper 200 m only and that the depth scale of panels a–e is non linear. Produced with Ocean Data View (Schlitzer, 2017).

$$N_j = \sum_j x_{ij} \cdot \alpha_i \quad (6)$$

where α_i is the linear fitting parameter of WT i for parameter N. The determination coefficient (R^2) and the standard deviation of the residuals (SD res) of this regression define the goodness of the fit.

2.4.3. Mixing–biogeochemical model of DOC and CDOM

The distribution of any chemical variable depends on (i) the conservative mixing of water masses with contrasting initial values of that chemical variable and (ii) the non–conservative biogeochemical processes occurring during that mixing. The non–conservative processes can be classified in two types: those that correlate with the water mass proportions and those that are independent of the water mass proportions.

The non–conservative processes that correlate with the water mass proportions represent the mineralization occurring from the area of formation of each water mass to the study transect. Therefore, the multiple linear regressions with the water type proportions (Eq. (6)) do not retain only the variability due to mixing of water masses of contrasting origins and initial concentrations of the chemical properties. They retain also the variability associated with the biogeochemical processes occurring at the basin–scale (Pérez et al., 1993; Álvarez-Salgado et al., 2013; Álvarez et al., 2014). In our particular case, basin-scale means the whole MedSea, including the formation areas of all the Mediterranean water masses. By contrast, the non–conservative processes independent of the water mass proportions retain the variability associated to the biogeochemical processes occurring at the local-scale. In our case, since the HOTMIX 2014 cruise covered a substantial part of the MedSea, the non–conservative processes independent of the water mass proportions are representative of the MedSea out of the deep water mass formation areas.

Simultaneous modelling of the impact of both mixing and biogeochemical processes on the distribution of DOC and CDOM implies the addition to Eq. (6) of a term that models the non–conservative processes independent of the water type proportions. To do that, an explanatory chemical variable (N_2) is introduced to improve our explanation of the response variable (N_1) as follows:

$$N_{1j} - \sum_j x_{ij} \cdot \alpha_{1i} = \beta \cdot \left(N_{2j} - \sum_j x_{ij} \cdot \alpha_{2i} \right) \quad (7)$$

Note that the term in the left represents the residuals of Eq. (6) for the response variable and the term in parenthesis in the right are the residuals of Eq. (6) for the explanatory variable. β is the fitting parameter of the relationship between N_1 and N_2, independent of the mixing, assuming that such a relationship is linear and homogeneous (i.e., β does not vary) in all the study area. This equation can be rearranged as follows:

$$N_{1j} = \sum_j x_{ij} \cdot (\alpha_{1i} - \beta \cdot \alpha_{2i}) + \beta \cdot N_{2j} \quad (8)$$

Therefore, a system of n linear equations (one per sample) with m + 1 unknowns (one per water type, $\alpha_{1i} - \beta \cdot \alpha_{2i}$, and the coefficient β) has to be solved. As for the case of Eq. (6), the goodness of this linear mixing–biogeochemical model was tested using the determination coefficient (R^2) and the standard deviation of the residuals of the least squares analysis (SD res).

3. Results

3.1. Distribution of the main MedSea water masses during the HOTMIX cruise

The distributions of the variables used to run the OMP analysis (salinity, potential temperature, NO and silicate) are presented in Fig. 2.

Salinity in the upper layers mainly reflects the shallow overturning cell of the MedSea with the low salinity surface Atlantic Water (AW) displacing from West to East, centred at 88 ± 14 m in the WestMed and 125 ± 26 m in the EastMed (Table 3; Fig. 3). Note that in the EastMed the AW is introduced in the OMP Analysis as modified Atlantic Water (MAW) (Table 1a). In the Levantine basin, the MAW mixes with the Levantine Surface Water (LSW), centred at 116 ± 21 m (Table 3; Fig. 3). These shallow water masses represent all together 8.7% of the total volume sampled during the cruise (Table 3). The counterpart of this low salinity eastward surface flow is the high salinity Levantine Intermediate Water (LIW) that returns at depth towards the Atlantic. Maximum salinity was found around 200 m in the EastMed (Fig. 2a). LIW is centred at 149 ± 13 m in the EastMed, where it represents

Table 3
Archetypal depth (Z_i), apparent oxygen utilization (AOU_i), dissolved organic carbon (DOC), absorption coefficient at 254 nm (a_{254i}) and 325 nm (a_{325i}), slope between 275 and 295 nm ($S_{275–295i}$), slope between 350 and 400 nm ($S_{350–400i}$), ratio of the slope between 275 and 295 nm divided by the slope between 350 and 400 nm (S_{Ri}), and the prokaryotic heterotrophic abundance (PHA) of the water masses intercepted during the HOTMIX cruise. The percentage of the total volume of water sampled corresponding to each water type (VOL_i) is also reported.

	Acronym	VOL_i (%)	Z_i (m)	AOU_i (μmol kg^{-1})	DOC_i (μmol L^{-1})	a_{254i} (m^{-1})	a_{325i} (10^{-2} m^{-1})	$S_{275–295i}$ (μm^{-1})	S_{Ri}	PHA_i (10^{-3} cells ml^{-1})
EastMed	MAW	3.2	125 ± 26	13 ± 5	57 ± 3	1.16 ± 0.05	18.1 ± 1.4	33.3 ± –1.4	2.2 ± 0.1	348 ± 53
	LSW	1.8	116 ± 21	3 ± 3	59 ± 2	1.18 ± 0.06	15.3 ± 0.8	37.3 ± –1.5	2.5 ± 0.2	331 ± 50
	LIW	12.2	149 ± 13	15 ± 2	59 ± 1	1.08 ± 0.03	15.0 ± 0.5	35.8 ± –0.5	2.4 ± 0.1	260 ± 18
	CIW	6.6	379 ± 56	47 ± 3	48 ± 2	0.86 ± 0.03	12.6 ± 0.6	33.4 ± –0.8	2.6 ± 0.1	122 ± 15
	AdMW	5.8	273 ± 55	34 ± 5	54 ± 2	0.94 ± 0.05	13.7 ± 0.9	33.9 ± –0.9	2.4 ± 0.1	179 ± 27
	AdDW	0.5	1425 ± 403	59 ± 4	41 ± 1	0.65 ± 0.02	9.5 ± 0.6	30.7 ± –3.6	2.3 ± 0.3	42 ± 8
	Pre–EMT	14.3	1462 ± 125	62 ± 1	39 ± 1	0.66 ± 0.01	9.6 ± 0.3	32.3 ± –0.5	2.5 ± 0.1	41 ± 4
	EMT	4.3	1702 ± 135	62 ± 1	37 ± 1	0.62 ± 0.01	8.6 ± 0.3	33.6 ± –1.1	2.5 ± 0.1	30 ± 3
	Post–EMT–A	3.3	1903 ± 180	58 ± 1	40 ± 1	0.65 ± 0.01	9.3 ± 0.3	32.5 ± –1.2	2.4 ± 0.1	32 ± 3
	Post–EMT–B	2.3	2892 ± 227	55 ± 1	41 ± 1	0.66 ± 0.01	9.8 ± 0.3	31.6 ± –1.0	2.2 ± 0.1	31 ± 3
	Post–EMT–C	1.8	2414 ± 235	56 ± 1	41 ± 1	0.66 ± 0.01	9.9 ± 0.3	31.1 ± –1.3	2.3 ± 0.1	30 ± 4
WestMed	AW	3.7	88 ± 14	23 ± 5	56 ± 2	1.11 ± 0.03	19.3 ± 0.9	30.7 ± –0.4	2.1 ± 0.0	550 ± 60
	EIW	11.4	364 ± 79	51 ± 5	50 ± 1	0.89 ± 0.03	15.1 ± 0.7	30.3 ± –0.2	2.3 ± 0.0	308 ± 45
	WIW	6.9	170 ± 33	45 ± 5	53 ± 1	0.99 ± 0.03	17.2 ± 0.8	30.0 ± –0.3	2.3 ± 0.0	414 ± 53
	A	9.3	1210 ± 156	67 ± 1	42 ± 1	0.69 ± 0.01	11.2 ± 0.3	28.9 ± –0.3	2.4 ± 0.0	86 ± 13
	B	5.8	1632 ± 222	61 ± 2	43 ± 1	0.69 ± 0.01	10.9 ± 0.3	29.0 ± –0.3	2.5 ± 0.1	77 ± 12
	C	0.7	2012 ± 300	56 ± 1	42 ± 2	0.67 ± 0.01	10.4 ± 0.5	29.5 ± –1.1	2.5 ± 0.2	51 ± 3
	D11	0.7	2476 ± 357	55 ± 1	42 ± 2	0.69 ± 0.01	10.8 ± 0.4	29.2 ± –1.2	2.4 ± 0.2	55 ± 4
	D14	5.4	2134 ± 160	56 ± 1	42 ± 1	0.68 ± 0.00	10.7 ± 0.2	28.9 ± –0.5	2.4 ± 0.1	56 ± 2

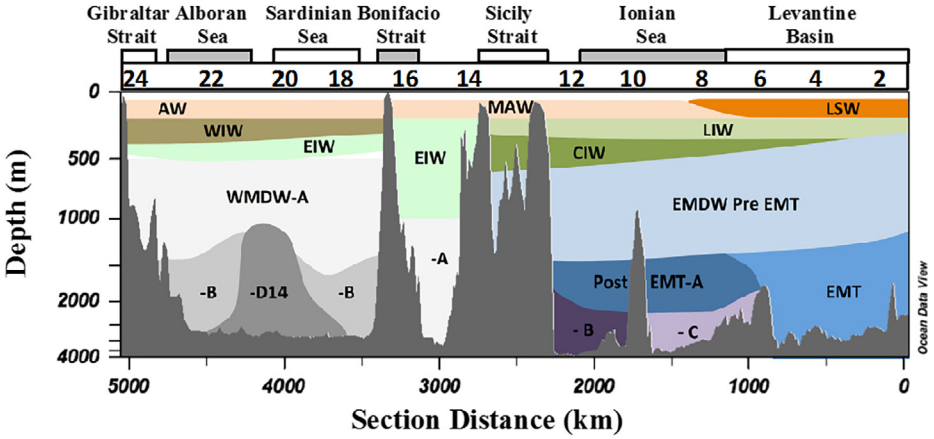

Fig. 3. Distribution of the water masses in the MedSea. See Table 1 for detailed information of the water masses nomenclature. Note that the depth scale is non linear.

12.2% of the total volume of water sampled during the cruise (Table 3). In the WestMed, a modified LIW, named as Eastern Intermediate Water (EIW) is introduced in the OMP analysis (Table 1b). Note that the EIW is a mixture of the LIW that enters the WestMed through the Sicily Strait, with WIW and the Ionian deep water (Table 1b). EIW is centred at 364 ± 79 m and represents 11.4% of the volume sampled (Table 3). In the EastMed, where the LIW is shallower, it is also important the volume of Cretan Intermediate Water (CIW), 6.6% of the volume sampled, that forms in the Cretan Sea and spreads below the LIW at 379 ± 56 m (Table 3; Fig. 3). Conversely, in the WestMed, where the EIW is deeper, the layer above this water mass is occupied by the Winter Intermediate Water (WIW), formed in the Western Mediterranean basin, centred at 170 ± 33 m and representing 6.9% of the total volume sampled (Fig. 3).

Similarly to salinity, θ presented its maximum in the upper layers of the EastMed (Fig. 2b), reaching a θ_i of 17.8 °C (Table 2) for the LSW. In the EastMed, the average ± SD of θ in the surface layer was 16.17 ± 0.78 °C, whereas in the WestMed the value was lower, 13.99 ± 0.35 °C. In the deep layers, different varieties of EMDW, with initial salinites ranging from 38.717 to 38.788 and initial temperatures from 13.40 to 13.64 °C, were found (Table 2). They were more saline and warmer than the varieties of WMDW found in the WestMed, which ranged from 38.460 to 38.492 and 12.840 to 12.913 °C (Table 2). The Pre–EMT water type is the most abundant EMDW sampled during the cruise, with 14.3% of the total volume and it is located at 1462 ± 125 m depth (Table 3; Fig. 3); the EMT water type is present in the Levantine basin just below the Pre–EMT water at a depth of 1702 ± 135 m (Fig. 3). The Post–EMT, with three different varieties (A, B, C), is the most recent EMDW water mass produced in the Adriatic Sea after the EMT event. The Post–EMT–A was intercepted in the Levantine basin just below EMT, at 1903 ± 180 m, representing 3.3% of the total volume. The Post–EMT–B and Post–EMT–C were intercepted in the Ionian Sea, i.e. much closer to their formation area, at depths > 2000 m near Crete, covering a lower volume extent (2.3 and 1.8% of the total volume, respectively). These youngest water masses are replacing and uplifting the old water masses present in this basin. In the deep WestMed, WMDW is formed in winter in the Gulf of Lions (Gascard, 1978) and occupies the water column below the EIW (Fig. 3). Here, five different varieties of WMDW have been intercepted. The variety A is the oldest and the most abundant deep WT of the WestMed, with 9.3% of the total sampling volume; the varieties B and C were originated in winter 2004/5 but they presented different θ–S properties, implying a larger contribution of LIW to B and of AW to C (Schroeder et al., 2006). The most recent varieties, D11 and D14, were found in 2011 and 2014 and correspond to the saltiest and densest WMDW (Puig et al., 2013; Schroeder et al., 2016; Houpert et al., 2016).

NO ranged between 220 and 300 μmol kg^{-1} and its maximum was found in the deep waters of the WestMed (Fig. 2c) indicating the presence of the newest variety of the WMDW (WMDW–D) which is characterized by the maximum initial NO value of 280 ± 5 μmol kg^{-1} (Table 2). SiO_4 ranged between 0.6 and 9.6 μmol kg^{-1} (Fig. 2d). The highest SiO_4 concentrations were found in the deep waters of the WestMed, with SiO_{4i} values around 9.5 μmol kg^{-1} (Table 2). In the EastMed, the highest SiO_4 concentrations were found at about 1000 m in the Levantine basin, where the Pre–EMT with an initial SiO_4 of 9.1 μmol kg^{-1} (Table 2) is found. In the upper ocean, low SiO_4 concentrations of around 2 μmol kg^{-1} covered a thick depth range in the EastMed up to 400 m, whereas in the WestMed higher SiO_4 values for the same depths were observed as a result of the AW inflow (Fig. 2d).

3.2. Distribution of the explanatory variables: AOU and Chl a

The distribution of AOU in the MedSea during the HOTMIX cruise (Fig. 2e) reflects the differential ageing of the 19 water types intercepted during the navigation, i.e. the cumulative oxygen consumption from the area of formation of each water mass to the study section. The lowest AOU levels were recorded in the epipelagic layer (< 150 m) with a significant decrease towards the East (Fig. 2e). Whereas the AW of the WestMed had an archetype AOU of 23 ± 5 μmol kg^{-1}, the LSW formed in the Levantine basin was characterized by an archetype AOU of just 3 ± 3 μmol kg^{-1} (Table 3). AOU values were maxima in the mesopelagic layer (150–1000 m) all along the MedSea, increasing towards the West as in the surface layer. The LIW was characterized by an archetype AOU of 15 ± 2 μmol kg^{-1} whereas this value was 51 ± 5 μmol kg^{-1} for the EIW. The other intermediate waters of the WestMed (WIW) and EastMed (CIW) had the same archetype AOU of 45–47 μmol kg^{-1} (Table 3). Furthermore, the AOU maximum layer was shallower in the WestMed, between 350 and 400 m, concurring with the archetype depth of the EIW (364 ± 79 m) (Table 3; Fig. 2e) as was previously observed (Álvarez et al., 2014; Tanhua et al., 2013). Note that although the AOU maximum in the WestMed reached up to 80 μmol kg^{-1}, the archetype AOU of the EIW was 51 ± 5 μmol kg^{-1} because it is a water mass proportion weighted average of all samples containing EIW and not just those from the AOU maximum. In the EastMed, the AOU maximum was found deeper, between 600 and 700 m, in between the LIW, centred at 149 ± 13 m and the Pre–EMT, centred at 1462 ± 125 m (Table 3). Finally, in the bathypelagic layer (> 1000 m) the older EMDW varieties, present in the Levantine basin, had a higher archetype AOU of 62 ± 1 μmol kg^{-1}. In contrast, the younger EMDW branches, found in the Ionian Sea, had a lower AOU of 55–58 μmol kg^{-1}. In the western basin, the oldest WMDW–A presented the highest archetype AOU of 67 ± 1 μmol kg^{-1} whereas the youngest varieties (WMDW–B, C, D) had a lower AOU of 55–61 μmol kg^{-1} (Table 3).

Apart from the AOU, which is a key parameter to understand the distribution of any biogeochemical variable throughout the entire water column, Chl *a* is also a major environmental driver in the epipelagic layer of the ocean. In the MedSea, as in any other oligotrophic region, Chl *a* levels are very low and concentrated around a DCM. This DCM was shallower and with higher Chl *a* concentrations in the oligotrophic WestMed than in the ultraoligothropic EastMed (Fig. 2f). In the EastMed, the DCM was situated at 93 ± 11 m with a mean ± SD concentration of 0.22 ± 0.08 mg m^{-3} and in the WestMed was at 53 ± 18 m with 0.46 ± 0.17 mg m^{-3}.

3.3. Distributions of the response variables: DOC and CDOM

In the epipelagic layer, the EastMed showed higher DOC concentrations than the WestMed (Fig. 4a), with mean ± SD values of 60 ± 1 and 56 ± 1 µmol L^{-1}, respectively. In fact, the water mass with the highest archetype DOC concentration was the LSW with 59 ± 2 µmol L^{-1} (Table 3). In the mesopelagic layer, a marked westward decrease of DOC was observed with the LIW presenting an archetype DOC of 59 ± 1 µmol L^{-1}, whereas the EIW presented 50 ± 1 µmol L^{-1}. Accordingly, DOC removal occurs when this water mass moves westwards. Unlike the epi– and mesopelagic layers, DOC

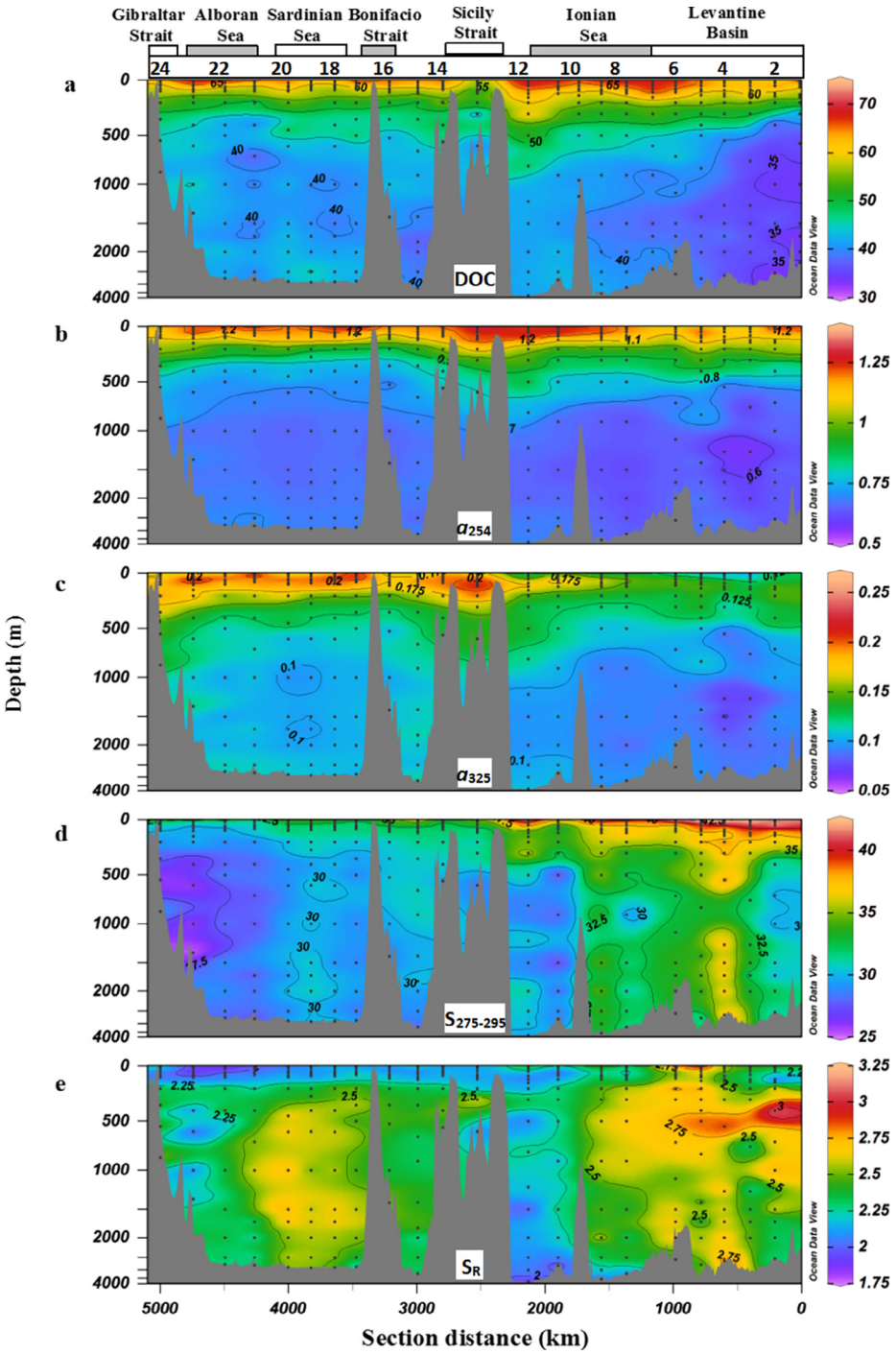

Fig. 4. Distribution of (a) DOC (µmol C L^{-1}), (b) absorption coefficient at 254 nm (a_{254}, m^{-1}), (c) absorption coefficient at 325 nm (a_{325}, m^{-1}), spectral slope between 275 and 295 nm ($S_{275–295}$, μm^{-1}), and (d) slope ratio (S_R, unitless). Note that the depth scale of panels a–e is non linear. Produced with Ocean Data View (Schlitzer, 2017).

concentrations in the bathypelagic layer (> 1000 m) were much lower and homogeneous. Most of the deep water masses of the EastMed and WestMed present archetype concentrations of 39–41 and 42–43 μmol L^{-1}, respectively (Table 3). It is remarkable the low archetype DOC of the EMDW formed during the EMT (37 ± 1 μmol kg^{-1}).

a_{254} values ranged between 0.56 to 1.34 m^{-1} and maximum values were found in the epipelagic layer, particularly in the Ionian Sea (Fig. 4b). As for the case of DOC, the LSW presented the maximum archetype a_{254} value of 1.18 ± 0.06 m^{-1}, followed by the MAW with 1.16 ± 0.05 m^{-1} (Table 3). The lowest values were found around 1500 m in the EastMed and the minimum archetype a_{254} was attributed to the EMT (0.62 ± 0.01 m^{-1}). Overall, the distribution of a_{254} (Fig. 4b) was parallel to the distribution of DOC (Fig. 4a); the direct linear regression of both variables was highly significant (DOC = 9 (± 1) + 46 (± 1)·a_{254}; R^2 = 0.87, p < 0.001, n = 273; Fig. 5).

For a_{325}, minimum values were also found in the deep waters of the EastMed (Fig. 4c), and the lowest archetype a_{325} was attributed again to the EMT with 8.6 ± 0.3 × 10^{-2} m^{-1} (Table 3). In the epipelagic layer, a_{325} decreased from West to East, from archetype values of 19.3 ± 0.9 × 10^{-2} m^{-1} for the AW to 15.3 ± 0.8 × 10^{-2} m^{-1} for the LSW (Table 3). Considering the $S_{275–295}$ and the S_R ratio, the largest values were found in the EastMed at around 500 m depth (Fig. 4d and e). The LSW features the highest archetype $S_{275–295}$ of 37.3 ± 1.5 μm^{-1} and the CIW the highest S_{Ri} of 2.6 ± 0.1 (Table 3). Whereas the lowest $S_{275–295}$ values were found in the WestMed between 500 and 1500 m (Fig. 4d) with minimum archetype $S_{275–295}$ for the five WMDW varieties, the S_R values were more spreaded over the WestMed surface and the deep layer of the Ionian Sea (Fig. 4e). The lowest ratio was found in the AW with a value of 2.1 ± 0.1.

3.4. Results of GAM analysis in the epipelagic waters of the MedSea

We used GAMs for exploring non–linear relationships between CDOM parameters and selected environmental factors (Fig. 6). The variable that exhibited the largest effect on DOC was AOU (F–value = 85.73; Table S2) with a negative power–law relationship (Fig. 6a) and a percentage of the variance explained of 51.1%. Likewise, a_{254} had AOU as the most significant explanatory variable (F–value = 52.07; Table S3) with a negative linear relationship (Fig. 6b). For a given AOU, any increase in θ has a negative effect on a_{254} (F–value = 10.68; Table S3; Fig. 6b). However, a_{254} responded positively to PHA until reaching a concentration of approximately e^{13} (= 4.4·10^5 cell mL^{-1}; F–value = 4.94; Table S3). All these three variables together presented a deviance explained (DE) of 76.2% (Table S3).

Contrary to a_{254}, a_{325} was mainly controlled by θ (F–value = 56.79; Table S3), decreasing its value linearly with increasing temperature (Fig. 6c). For a given θ, a_{325} presented a negative power–law response to AOU (F–value = 11.22) with a plateau at around 20 μmol kg^{-1} (Fig. 6c). Unlike a_{254}, PHA presented a positive linear relationship with a_{325} from values of $e^{12.7}$ (= 3.3·10^5) cell mL^{-1} onwards at a constant AOU value (F–value = 11.86). In this case, Chl *a* contributed significantly to explain a_{325} in contrast with a_{254} (F–value = 8.60), being positive until becoming constant at a value of e^{-2} (= 0.14) mg m^{-3}. These four variables contributed to explain 72.6% of the total variance of a_{325}. Similarly, $S_{275–295}$ was explained by the same variables than a_{325} at a DE = 83% (Table S3). In addition, it was mostly explained by θ (F–value = 56.88), through a positive linear relationship (Fig. 6d). Here, Chl *a* and bacterial abundance contributed more substantially to explain the variability of this parameter than those of the absorption coefficients, with F–values of 20.11 and 19.32, respectively (Table S3). At a given θ, bacterial abundance and AOU exert negatively at values higher than approximately $e^{12.7}$ (= 3.3·10^5) cell mL^{-1} and 20 μmol kg^{-1}, respectively. The explained variance for S_R (43.5%) was substantially lower than those of the absorption coefficients and $S_{275–295}$ (Table S3). S_R variability was controlled by θ, AOU and Chl *a* with F–values of 18.74, 20.02 and 15.23 (Table S3). Whereas the relationship with θ was positive and linear, the relationships with AOU and Chl *a* were not, shifting from positive to negative at AOU of around 30 μmol kg^{-1} and from negative to positive for Chl *a* at around e^{-2} (= 0.14) mg m^{-3} (Fig. 6e).

3.5. Mixing and biogeochemical model results for the meso– and bathypelagic waters of the Mediterranean Sea

The mixing model (Eq. (6)), which includes the effect of water mass mixing and basin–scale mineralization, explained 83% of the variability of DOC in the meso– and bathypelagic MedSea (Table 4). The addition of AOU produces a mixing–biogeochemical model (Eq. (7)) that increased the explained variability to 86%, accompanied by a SD res reduction of 10.3% (Table 4). The water mass mixing independent DOC/AOU slope for the entire MedSea was −0.22 ± 0.03 mol C mol O_2^{-1}, which translates into a DOC/AOU–Ceq ratio of 31 ± 4% assuming a -O_2/C mineralization ratio of 1.4 (Anderson and Sarmiento 1994, Anderson, 1995). In the EastMed, the mixing model explained 86% of the variability of DOC, which increased to 90% when AOU is included in the mixing–biogeochemical model and SD res reduced by 15.2% (Table 4). For this basin, the slope DOC/AOU slope was −0.47 ± 0.07 mol C mol O_2^{-1}, i.e. a DOC/AOU–Ceq ratio of 66 ± 10%. Conversely, in the WestMed, the mixing model explained much less variability (only 74%), which increased to 80% when AOU is included and the resultant DOC/AOU slope was −0.17 ± 0.03 mol C mol O_2^{-1}, which translates into a DOC/AOU–Ceq ratio of 24 ± 4%. For the case of a_{254}, the mixing model explained 91% of its variance in the entire MedSea. Inclusion of AOU derives in a mixing–biogeochemical model that increased the explained variance of a_{254} to 95% with a substantial SD res reduction by 26.3%. In the WestMed, the SD res reduction was even higher (i.e. 38.4%, Table 4). The water mass mixing independent a_{254}/AOU ratio was significantly higher in the EastMed (−8 (± 1) 10^{-3} m^{-1} kg^{-1} μmol O_2^{-1} or −8 ± 1 m^2 mmol O_2^{-1}) than in the WestMed (−4.3 (± 0.4) 10^{-3} m^{-1} kg^{-1} μmol O_2^{-1} or −4.3 ± 0.4 m^2 mmol O_2^{-1}).

The mixing model explained 82% of the variability of a_{325}, increasing to 88% when adding the AOU as explanatory variable in the mixing–biogeochemical model. Furthermore, a SD res reduction of 17.8% was observed. In this case, a maximum SD res reduction of 25.5% was observed in the WestMed (Table 4). Unexpectedly, a_{325} decreased with basin scale mineralization (Fig. 7a); the water mass mixing independent a_{325}/AOU slope was negative, −1.0 (± 0.1) 10^{-3} m^{-1} kg μmol O_2^{-1} (or −1.0 ± 0.1 m^2 mmol O_2^{-1}), for the entire

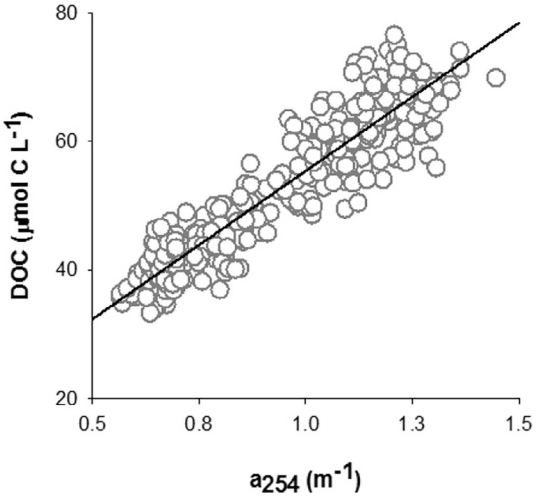

Fig. 5. Relationship of DOC (μmol C L^{-1}) with a_{254i} (m^{-1}).

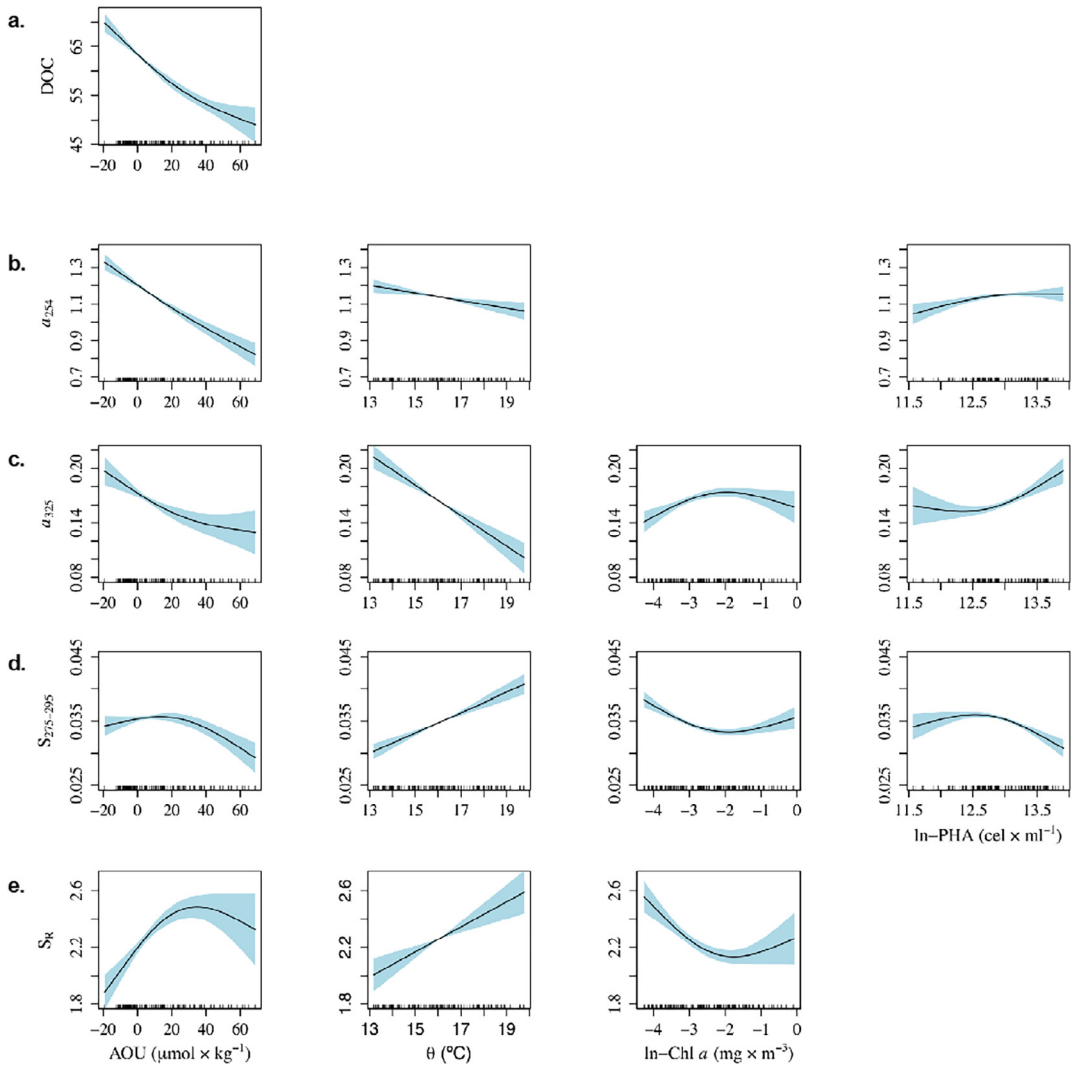

Fig. 6. Partial plots of the additive effects of the physical, chemical and biological covariates on the DOC and CDOM parameters after fitting Generalized Additive Models. (a) DOC (μmol C L^{-1}), (b) a_{254} (m^{-1}), (c) a_{325} (m^{-1}), (d) $S_{275–295}$ (μm^{-1}). (e) S_R (unitless). Ticks on x-axis indicate the distribution of the data.

MedSea, with no significant differences among basins. Water mass mixing explained much less variance of $S_{275–295}$ (64%) and there was not any improvement when considering the mixing–biogeochemical model (Table 4).

Finally, S_R was the CDOM parameter with less percentage of explained variance by the linear mixing model with 35% (Table 4). Consideration of the mixing–biogeochemical model contributed scarcely to increase the explained variance, even for the two basins separately (Table 4). Interestingly, the water mass mixing independent S_R/AOU ratio was positive, 6 (± 2) 10^{-3} kg μmol $O_2{}^{-1}$ (or 6 ± 2 m^3 mmol $O_2{}^{-1}$), being higher in the EastMed, 17 (± 6) 10^{-3} kg μmol $O_2{}^{-1}$ (or 17 (± 6) m^3 mmol $O_2{}^{-1}$.

Only for a_{254} and a_{325}, the simultaneous inclusion of AOU and PHA in the mixing–biogeochemical model improved the explained variance and reduced the SD res (not shown). In the entire MedSea, for a_{254}, the explained variance increased to 96% and the SD res reduced by 27.3% compared with the mixing model. For a_{325}, the explained variance and SD res reduction were 89% and by 21.4%, respectively. In the WestMed, the SD res reduction was even higher, reaching 41.2% and 29.1% for a_{254} and a_{325}, respectively. In the EastMed, no improvement with the addition of PHA was detected. It is northworthy to underscore the positive relationship of PHA with both absorption coefficients, contrary to the negative relationship recorded with AOU.

4. Discussion

4.1. DOM, a major player in the carbon cycle of the Mediterranean Sea

Despite the relatively small size of the MedSea and the short renewal times of the western (42 years) and eastern (150 years) Mediterranean deep waters (Powley et al., 2016), DOC concentrations in the deep MedSea expand over the range found in the deep waters of the World Ocean, from 34 to 45 μmol L^{-1} (Table 3; Fig. 4a). Whereas the average DOC concentration of the WMDW varieties is around 42–43 μmol L^{-1}, it drops to 37–41 μmol L^{-1} in the less ventilated EMDW varieties. Particularly, the archetype DOC concentration of the EMT, 37 ± 1 μmol L^{-1}, is similar to the concentration found in the North Pacific Intermediate Water (NPIW), which is among the less ventilated water masses of the world ocean (Hansell et al., 2009; 2012). Note that the EMT is an old water mass, but not the oldest of the EastMed, which is the Pre–EMT with an archetype DOC of 39 ± 1 μmol L^{-1}. Given that the archetype AOU of both water masses is the same, 62 ± 1 μmol kg^{-1} (Table 3), the 2 μmol L^{-1} difference in archetype DOC should be due to the different initial DOC concentrations of these water masses at their respective formation site in the Aegean Sea (during the EMT) or in the Ionian Sea (before the EMT).

The DOC distribution obtained in our study is consistent with previous ones in the MedSea (Santinelli et al., 2010; Santinelli, 2015). The

Table 4
Parameters of the linear mixing (Eq. (6)) and mixing–biogeochemical (Eq. (7)) models. R^2, determination coefficient; SD res, standard deviation of the residuals of the estimation; % SD reduction, percentage of reduction of the SD res of the mixing biogeochemical as compared with the corresponding mixing model; β, fitting parameter of the relationship between N_1 and N_2 independent of the mixing; SE(β), standard error of the estimation of β; *p*, significance level of the estimation of β. Results are presented for all samples (a) and for the Eastern (b) and Western (c) basins.

N_1	N_2	R^2	SD res	%SD reduction	β	SE(β)	*p*	n
MedSea								
AOU		0.88	7.8					233
HPA		0.78	88,518					240
DOC		0.83	3.8					233
a_{254}		0.91	0.06					209
a_{325}		0.82	0.02					209
$S_{275–295}$		0.64	0.002					209
S_R		0.35	0.2					149
DOC	AOU	0.86	3.4	10.3%	−0.22	0.03	0.0000	226
a_{254}	AOU	0.95	0.05	26.3%	−0.0048	0.0004	0.0000	203
a_{325}	AOU	0.88	0.01	17.8%	−0.0010	0.0001	0.0000	203
$S_{275–295}$	AOU	0.64	0.002	−0.5%			n.s.	203
S_R	AOU	0.37	0.2	2.1%	0.006	0.002	0.0012	203
EastMed								
AOU		0.96	4.4					130
HPA		0.85	51,696					134
DOC		0.86	3.9					131
a_{254}		0.92	0.06					105
a_{325}		0.84	0.01					105
$S_{275–295}$		0.46	0.002					105
S_R		0.34	0.2					105
DOC	AOU	0.90	3.3	15.2%	−0.47	0.07	0.0000	126
a_{254}	AOU	0.95	0.05	21.0%	−0.008	0.001	0.0000	101
a_{325}	AOU	0.85	0.01	7.4%	−0.0007	0.0003	0.0270	101
$S_{275–295}$	AOU	0.43	0.002	−1.3%			n.s.	101
S_R	AOU	0.36	0.2	2.8%	0.017	0.006	0.0056	101
WestMed								
AOU		0.72	10.6					103
HPA		0.73	119,600					106
DOC		0.74	3.6					102
a_{254}		0.90	0.06					104
a_{325}		0.80	0.02					104
$S_{275–295}$		0.31	0.001					104
S_R		0.35	0.2					104
DOC	AOU	0.80	3.2	10.9%	−0.17	0.03	0.0000	99
a_{254}	AOU	0.96	0.04	38.4%	−0.0043	0.0004	0.0000	101
a_{325}	AOU	0.89	0.01	25.5%	−0.0010	0.0001	0.0000	101
$S_{275–295}$	AOU	0.31	0.001	0.8%			n.s.	101
S_R	AOU	0.41	0.2	3.6%	0.005	0.002	0.00705	101

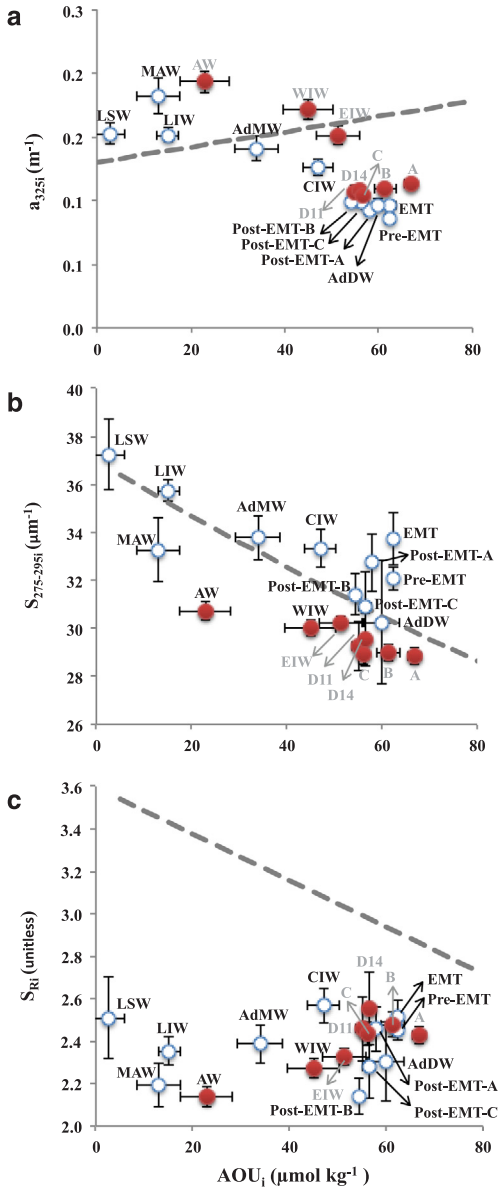

Fig. 7. Relationships of archetype (a) a_{325i} (m^{-1}), (b) $S_{275–295i}$ (µm^{-1}) and (c) S_{Ri} (unitless) with archetype apparent oxygen utilization (AOU$_i$, µmol kg^{-1}). Error bars represent the standard deviation of the estimated archetypal values. Red and white circles represent samples of the western and eastern basins, respectively. The acronyms of the water masses are explained in Table 1. The dashed grey lines represent the regression curves found by Catalá et al. (2015) for the global ocean. (For interpretation of the references to colour in this figure legend, the reader is referred to the web version of this article.)

novelty of this work has been the application of a water mass analysis that allowed us to obtain water mass proportion weighted–average DOC concentrations for each of the 19 water types identified during the HOTMIX cruise.

An additional advantage of the water mass analysis is the possibility of estimating the contribution of DOC to the dissolved oxygen demand of the dark MedSea independent of water mass mixing. The values of parameter β in the DOC–AOU mixing biogeochemical model (Table 4), indicate that 66 ± 10% of the oxygen demand of the dark Eastern basin and 24 ± 4% in the dark Western basin is due to DOC consumption. For the whole dark MedSea, the contribution of DOC is 31 ± 4%. Previous estimates by Santinelli et al. (2010, 2012) for the core of the LIW indicated a contribution of around 49 ± 4% during its route across the Ionian and Tyrrhenian Sea and 32 ± 4% when the whole MedSea is considered. Therefore, when considering the whole meso– and bathypelagic EastMed, the contribution of DOC to the oxygen demand is much higher than when considering only the core of the LIW. This excess consumption is likely due to the injection of bioavailable DOC accumulated in the surface layer (< 50 m) into the winter mixed layer (< 150 m) all along the EastMed, as described by Carlson et al. (1994) for the Sargasso Sea.

As indicated above, our results also show an accumulation of DOC in the surface layer of the EastMed in agreement with previous studies (Pujo-Pay et al., 2011; Santinelli, 2015). The explanation behind this accumulation is that ultraoligotrophy decreases heterotrophic growth, resulting in a decoupling between DOC production and consumption (Thingstad et al., 1997; Pujo-Pay and Conan, 2003; Luna et al., 2012). DOC removal occurs after winter mixing through the winter mixed layer (< 150 m) and as the recently formed LIW (> 200 m) moves westwards, indicating DOC consumption as nutrients become more available.

4.2. Biogeochemistry of CDOM in the MedSea

Although both a_{254} and a_{325} are used as proxies of the concentration of CDOM in aquatic systems, they really represent different CDOM fractions. Whereas a_{254} is representative for the concentration of conjugated C double bonds (e.g. Lønborg and Álvarez-Salgado, 2014), a_{325} is representative for aromatic compounds (e.g. Jørgensen et al., 2014; Catalá et al., 2016). Aromaticity makes the latter compounds capable of absorbing UVB radiation, resulting in an increased susceptibility to photodegradation (Nelson et al., 2004; Catalá et al., 2015). For this reason, the GAMs analysis for the epipelagic layer, showed that a_{325} was basically controlled by temperature (Table S3, Fig. 6c). Water temperature has a well–known positive effect on microbial metabolic rates and it is a proxy for stratification and also for solar irradiation and, thus, for photobleaching (Fig. 6c). Consequently, the gradual decrease of a_{325} from West to East in the epipelagic layer can be explained by a combination of these factors. To a lesser extent, AOU, a proxy of the cumulative net community respiration (i.e., the community respiration minus the autotrophic oxygen production), also contributed to explain the decay of the aromatic substances represented by a_{325} (Fig. 6c). Conversely, the biological variables (Chl *a* and bacterial abundance) explained the generation of a_{325} up to a certain level (Fig. 6c). For a_{254}, the cumulative community respiration mostly explained the decay of this parameter.

In the meso and bathypelagic waters, the mixing model contributed to explain most of the variability of a_{254} and a_{325}. But consideration of the mixing–biogeochemical model for a_{254} and a_{325} reduced the SD res more substantially than for DOC (i.e. 26.3% and 17.8%, respectively), indicating that the local–mineralization processes play a larger influence on these CDOM parameters.

Spectral slopes have been commonly regarded as qualitative proxies of CDOM, providing information about its molecular weight and the content in aromatic substances (Helms et al., 2008). In the epipelagic layer, $S_{275–295}$ and S_R were mostly explained by θ, meaning that molecular weight is more affected by stratification/mixing and/or photobleaching processes than by the biological processes traced by AOU and Chl *a* (Table S3; Fig. 6d and e). Whereas photobleaching contribute to decrease the average molecular weight and the content in aromatic substances of CDOM, microbial activity counteracts increasing the molecular weight and aromaticity (Helms et al., 2008; Catalá et al., 2015; Maqbool et al., 2017). This would explain the higher absorption coefficient and average molecular weight of CDOM (i.e. lower $S_{275–295}$ and S_R) in parallel with the higher PHA in the WestMed than in the EastMed. The negative relationship between AOU and $S_{275–295}$ supports previous studies that found a decrease of the Helms's spectral slopes with water mass ageing in the dark global ocean (Catalá et al., 2015) (Fig. 7b).

4.2.1. a_{254} as a proxy for DOC

As in Lønborg and Álvarez-Salgado (2014) for the Northeast Atlantic Ocean, the highly significant linear regression of DOC with a_{254} in the MedSea (Fig. 5) confirms that a_{254} could be used as a proxy for the concentration of DOC. The intercept of this relationship indicates that 10 μmol L^{-1} of DOC varies independently of a_{254}, whereas the remaining variability would be dependent on a_{254}. The regression obtained by Lønborg and Álvarez-Salgado (2014) (DOC = 10 (± 1) + 40 (± 1) a_{254}; R^2 = 0.80; n = 233) presented a lower slope and the same intercept than that obtained for the MedSea in this work. Therefore, it seems that this relationship is not universal for the open ocean, and a site-specific equation is needed for each study area.

4.2.2. The counterintuitive behavior of a_{325} in the MedSea

Unlike other studies, an unexpected relationship between a_{325} and water mass ageing emerges in the MedSea. Whereas positive relationships between a_{325} and AOU have been observed in the global ocean, particularly in the Indian and Pacific oceans (Nelson et al., 2010; Catalá et al., 2015), here a_{325} decreases with increasing AOU both in the epipelagic (Fig. 6) and in the dark MedSea (Fig. 7a; Table 4). A positive relationship between a_{325} and AOU has been interpreted as a production of aromatic humic–like substances during microbial degradation of organic matter in the dark ocean (Nelson et al., 2010; Jørgensen et al., 2011; Catalá et al., 2015, 2016). Therefore, the negative a_{325}/AOU relationship obtained in the MedSea would suggest the prevalence of the consumption of the bulk CDOM absorbing at this wavelength over the microbial production of the fluorescent fraction of this CDOM. Accordingly, the positive S_R/AOU slope observed in the deep waters of the MedSea (particularly for $AOU_i > 30$ μmol kg^{-1}; Fig. 7c) is also contrary to what was observed in the global tropical and subtropical ocean (Catalá et al., 2015). Remarkably, S_R values in the MedSea are significantly lower than in the global ocean for the AOU range found in the MedSea (Fig. 7c), suggesting a larger influence of terrestrial CDOM in the enclosed MedSea (Helms et al., 2008).

We hypothesize that the dominance of CDOM consumption in the MedSea could be attributed to its oligotrophy, which would divert microbial heterotrophs towards a specialization in the consumption of colored compounds of more recalcitrant nature. However, as it will be further discussed in the companion paper by Martínez-Pérez et al. (this issue), the humic–like fluorescent fraction of the materials absorbing at 325 nm shows the expected increase with AOU.

5. Conclusions

In the epipelagic MedSea, AOU explained most of the variability of DOC and a_{254}, suggesting that the cumulative net community respiration is driving these two variables. However, the variability of a_{325}, $S_{275–295}$ and S_R was mostly explained by θ, a proxy to thermal stratification and solar radiation, indicating that apart from microbial activity, water column stability and photobleaching also drive the variability of CDOM.

For the meso– and bathypelagic MedSea, water mass mixing and basin–scale mineralization processes contributed more substantially to explain the variability of DOC, a_{254} and a_{325} (82–91%) than the variability of $S_{275–295}$ and S_R (35–64%). The addition of local mineralization processes only contributed to improve the explained variance of the absorption coefficients. Local mineralization processes also indicate that DOC and CDOM play a more relevant role in the carbon cycle of the EastMed than the WestMed: whereas DOC contributed to 66 ± 10% of the oxygen demand of the EastMed, it represented only 24 ± 4% in the WestMed.

a_{254} has revealed as an excellent proxy to the concentration of DOC in the MedSea and the overall negative relationship of a_{325} with AOU indicates that, contrary to expected, the consumption of colored substances absorbing at 325 nm prevails over their production.

Acknowledgements

We thank the Captain and crew of R/V Sarmiento de Gamboa. We appreciate the work of M.J. Pazó and V. Vieitez with DOC and inorganic nutrient analyses. We acknowledge the help of H. SanLeón–Bartolomé with the dissolved oxygen analysis and J. M. Gasol for his valuable comments to improve the manuscript. This work was funded by the project HOTMIX (grant number CTM2011–30010–C02–MAR) co–financed with FEDER funds. T.S.C. was supported by a predoctoral fellowship from the Ministry of Education, Culture y Sports (Ref. AP2009–2138), the project FOMEM (Spanish Research Council, CSIC–PIE No. 201030E130) and a postdoctoral contract jointly financed by the project CGL2014–52362R of the Spanish Ministry of Economy and Competitiveness and FEDER funds and the University of Granada. A.M.M. –P. was funded by a predoctoral fellowship from the Spanish Ministry of Economy and Competitiveness (Ref. BES–2012–056175) and the project MODMED (Spanish Research Council, CSIC–PIE No. 201730E020). M.N. –C. was supported by the project FERMIO

(MINECO, CTM2014–57334–JIN) co–financed with FEDER funds.

Contributions

T.S.C., X.A.A.–S. and J.A. designed the research. T.S.C., A.M.M.–P., M.N.–C., M.A., M.E., X.A. A.–S., J.A. participated in the field work. M. A. applied the water mass analysis. J.O. executed the GAM analysis. T.S.C. wrote the first draft manuscript, which was complemented by significant contributions of all co–authors.

Appendix A. Supplementary material

Supplementary data associated with this article can be found, in the online version, at https://doi.org/10.1016/j.pocean.2018.05.002.

References

Álvarez-Salgado, X.A., Nieto-Cid, M., Álvarez, M., Pérez, F.F., Morin, P., Mercier, H., 2013. New insights on the mineralization of dissolved organic matter in central, intermediate, and deep water masses of the northeast North Atlantic. Limnol. Oceanogr. 58, 681–696. http://dx.doi.org/10.4319/lo.2013.58.2.0681.

Álvarez, M., Brea, S., Mercier, H., Álvarez-Salgado, X.A., 2014. Mineralization of biogenic materials in the water masses of the South Atlantic Ocean. I: assessment and results of an optimum multiparameter analysis. Prog. Oceanogr. 123, 1–23. http://dx.doi.org/10.1016/j.pocean.2013.12.007.

Anderson, L.A., Sarmiento, J.L., 1994. Redfield ratios of remineralization determined by nutrient data analysis. Global Biogeochem. Cycles 8 (1), 65–80. http://dx.doi.org/10.1029/93GB03318.

Anderson, L.A., 1995. On the hydrogen and oxygen content of marine phytoplankton. Deep-Sea Res. Part I 42, 1675–1680. http://dx.doi.org/10.1016/0967-0637(95)00072-E.

Andrie, C., Merlivat, L., 1988. Tritium in the western Mediterranean Sea during 1981. Phycemed cruise. Deep-Sea Res. I 35, 247–267. http://dx.doi.org/10.1016/0198-0149(88)90039-8.

Arístegui, J., Duarte, C.M., Agustí, S., Doval, M., Álvarez-Salgado, X.A., Hansell, D.A., 2002. Dissolved organic carbon support of respiration in the dark ocean. Science 298 (5600), 1967. http://dx.doi.org/10.1126/science.1076746.

Artegiani, A., Gacic, M., Michelato, A., Kovacevic, V., Russo, A., Paschini, E., Scarazzato, P., Smircic, A., 1993. The Adriatic sea hydrography and circulation in spring and autumn (1985–1987). Deep Sea Res. Part II 40, 1143–1180. http://dx.doi.org/10.1016/0967-0645(93)90065-U.

Astraldi, M., Balopoulos, S., Candela, J., Font, J., Gacic, M., Gasparini, G., Manca, B., Theocharis, A., Tintoré, J., 1999. The role of straits and channels in understanding the characteristics of Mediterranean circulation. Prog. Oceanogr. 44, 65–108. http://dx.doi.org/10.1016/S0079-6611(99)00021-X.

Astraldi, M., Conversano, F., Civitarese, G., Gasparini, G.P., Ribera d'Alcalà, M., Vetrano, A., 2002. Water mass properties and chemical signature in the central Mediterranean region. J. Mar. Syst. 33–34, 155–177.

Azov, I., 1991. The Mediterranean Sea, a marine desert? Mar. Pollut. Bull. 23, 225–232. http://dx.doi.org/10.1016/0025-326X(91)90679-M.

Babin, M., Stramski, D., Ferrari, G.M., Claustre, H., Bricaud, A., Obolensky, G., Hoepffner, N., 2003. Variations in the light absorption coefficients of phyto– plankton, nonalgal particles, and dissolved organic matter in coastal waters around Europe. J. Geophys. Res. 108 (C7), 3211. http://dx.doi.org/10.1029/2001JC000882.

Bensi, M., Rubino, A., Cardin, V., Hainbucher, D., Mancero-Mosquera, I., 2013. Structure and variability of the abyssal water masses in the Ionian Sea in the period 2003–2010. J. Geophys.Res. Ocean. 118, 931–943. http://dx.doi.org/10.1029/2012JC008178.

Bergamasco, A., Malanotte-Rizzoli, P., 2010. The circulation of the Mediterranean Sea: a historical review of experimental investigations. Adv. Oceanogr. Limnol. 1 (1), 11–28. http://dx.doi.org/10.1080/19475721.2010.491656.

Bethoux, J.P., Tailliez, D., 1994. Deep–Water in the Western Mediterranean Sea, Yearly Climatic Signature and Enigmatic Spreading, in: Ocean Processes in Climate Dynamics: Global and Mediterranean Examples. Springer Netherlands, Dordrecht, pp. 355–369. http://doi.org/10.1007/978-94-011-0870-6_15.

Beuvier, J., Béranger, K., Lebeaupin-Brossier, C., Somot, S., Sevault, F., Drillet, Y., Bourdallé-Badie, R., Ferry, N., Lyard, F., 2012. Spreading of the Western Mediterranean Deep Water after winter 2005: time–scales and deep cyclone transport. J. Geophys. Res. 117, C07022. http://dx.doi.org/10.1029/2011JC007679.

Bricaud, A., Babin, M., Claustre, H., Ras, J., Tieche, F., 2010. Light absorption properties and absorption budget of Southeast Pacific waters. J. Geophys. Res. 115, C08009. http://dx.doi.org/10.1029/2009JC005517.

Bricaud, A., Roesler, C.S., Parslow, J.S., Ishizaka, J., 2002. Bio–optical studies during the JGOFS–equatorial Pacific program: a contribution to the knowledge of the equatorial system. Deep Sea Res. Part II 49, 2583–2599. http://dx.doi.org/10.1016/S0967-0645(02)00049-8.

Broecker, W.S., 1974. 'NO' a conservative water–mass tracer. Earth Planet. Sci. Lett. 23, 100–107. http://dx.doi.org/10.1016/0012-821X(74)90036-3.

Carlson, C.A., Ducklow, H.W., Michaelis, A.F., 1994. Annual flux of dissolved organic carbon from the euphotic zone in the northwestern Sargasso Sea. Nature 371, 405–408. http://dx.doi.org/10.1038/nature04158.

Carlson, C.A., Hansell, D.A., Nelson, N.B., Siegel, D.A., Smethie, W.M., Khatiwala, S., Meyers, M.M., Wallner, E., 2010. Dissolved organic carbon export and subsequent remineralization in the mesopelagic and bathypelagic realms of the North Atlantic basin. Deep-Sea Res. II 57 (16), 1433–1445. http://dx.doi.org/10.1016/j.dsr2.2010.02.013.

Catalá, T.S., Reche, I., Álvarez, M., Khatiwala, S., Guallart, E.F., Benítez-Barrios, V.M., Fuentes-Lema, A., Romera-Castillo, C., Nieto-Cid, M., Pelejero, C., Fraile-Nuez, E., Ortega-Retuerta, E., Marrasé, C., Álvarez-Salgado, X.A., 2015. Water mass age and aging driving chromophoric disolved organic matter in the dark global ocean. Global Biogeochem. Cy. 29. http://dx.doi.org/10.1002/2014GB005048.

Catalá, T.S., Álvarez-Salgado, X.A., Otero, J., Iuculano, F., Companys, B., Horstkotte, B., Romera-Castillo, C., Nieto-Cid, M., Latasa, M., Morán, X.A., Gasol, J.M., Marrasé, C., Stedmon, C.A., Reche, I., 2016. Drivers of fluorescent dissolved organic matter in the global epipelagic ocean. Limnol. Oceanogr. 61, 1101–1119. http://dx.doi.org/10.1002/lno.10281.

Cardin, V., Civitarese, G., Hainbucher, D., Bensi, M., Rubino, A., 2015. Thermohaline properties in the Eastern Mediterranean in the last three decades: Is the basin returning to the pre–EMT situation? Ocean Sci. 11, 53–66. http://dx.doi.org/10.5194/os-11-53-2015.

Emelianov, M., Font, J., Turiel, A., Millot, C., Solé, J., Poulain, P.–M., Julià, A., Vitrià, M.–R., 2006. Transformation of Levantine Intermediate Water tracked by MEDARGO floats in the Western Mediterranean, Ocean Sci. 2, 281–290. http://doi.org/10.5194/os-2-281-2006.

Gascard, J.C., 1978. Mediterranean deep water formation. Baroclinic instability and oceanic eddies. Oceanol. Acta 1, 315–330.

Gasparini, G.P., Ortona, A., Budillon, G., Astraldi, M., Sansone, E., 2005. The effect of the Eastern Mediterranean Transient on the hydrographic characteristics in the Strait of Sicily and in the Tyrrhenian Sea. Deep Sea Res. Part I 52, 915–935. http://dx.doi.org/10.1016/j.dsr.2005.01.001.

Grasshoff, K., Kremling, K., Ehrhardt, M., 1999. Determination of nutrients. In: L. Brügmann, L., Kremling, K. (Eds.). Methods of Seawater Analysis. WILEY–VCH Verlag GmbH, pp. 159–228.

Hainbucher, D., Rubino, A., Klein, B., 2006. Water mass characteristics in the deep layers of the western Ionian Basin observed during May 2003. Geophys. Res. Lett. 33, L05608. http://dx.doi.org/10.1029/2005GL025318.

Hansell, D.A., Carlson, C.A., Repeta, D.J., Reiner, S., 2009. Dissolved organic matter in the ocean. Oceanography 22, 202–211. http://dx.doi.org/10.5670/oceanog.2009.109.

Hansell D. A., Carlson, C. A., Schlitzer, R., 2012. Net removal of major marine dissolved organic carbon fractions in the subsurface ocean, Glob. Biogeochem. Cycles, 26, GB1016. http://doi.org/10.1029/2011GB004069.

Helms, J.R., Stubbins, A., Ritchie, J.D., Minor, E.C., Kieber, D.J., Mopper, K., 2008. Absorption spectral slopes and slope ratios as indicators of molecular weight, source, and photobleaching of chromophoric dissolved organic matter. Limnol. Oceanogr. 53, 955–969. http://dx.doi.org/10.4319/lo.2008.53.3.0955.

Holm-Hansen, O., Lorenzen, C.J., Holmes, R.W., Strickland, J.D., 1965. Fluorometric determination of chlorophyll. J. Cons. Int. Explor. Mer 30, 3–15.

Houpert, L., Durrieu de Madron, X., Testor, P., Bosse, A., D'Ortenzio, F., Bouin, M.N., Dausse, D., Le Goff, H., Kunesch, S., Labaste, M., Coppola, L., Mortier, L., Raimbault, P., 2016. Observations of open–ocean deep convection in the northwestern Mediterranean Sea: Seasonal and interannual variability of mixing and deep water masses for the 2007–2013 Period. J. Geophys. Res. Oceans 121, 8139–8171. http://dx.doi.org/10.1002/2016JC011857.

Huertas, I.E., Ríos, A.F., García–Lafuente, J., Navarro, G., Makaoui, A., Sánchez–Román, A., Rodriguez–Galvez, S., Orbi, A., Ruíz, J., Pérez, F.F., 2012. Atlantic forcing of the Mediterranean oligotrophy, Global Biochem. Cycles, 26, GB2022. http://doi.org/10.1029/2011GB004167.

Jørgensen, L., Stedmon, C.A., Kragh, T., Markager, S., Middelboe, M., Søndergaard, M., 2011. Global trends in the fluorescence characteristics and distribution of marine dissolved organic matter. Mar. Chem. 126, 139–148. http://dx.doi.org/10.1016/j.marchem.2011.05.002.

Jørgensen, L., Stedmon, C.A., Granskog, M.A., Middelboe, M., 2014. Tracing the long–-term microbial production of recalcitrant fluorescent dissolved organic matter in seawater. Geophys. Res. Lett. 41, 2481–2488. http://dx.doi.org/10.1002/2014GL059428.

Klein, B., Roether, W., Manca, B.B., Bregant, D., Beitzel, V., Kovacevic, V., Luchetta, A., 1999. The large deep water transient in the Eastern Mediterranean. Deep Sea Res. Part I 46, 371–414.

Klein, B., Roether, W., Kress, N., Manca, B.B., Ribera d'Alcala, M., Souvermezoglou, E., Theocharis, A., Civitarese, G., Luchetta, A., 2003. Accelerated oxygen consumption in eastern Mediterranean deep waters following the recent changes in thermohaline circulation. J. Geophys. Res. 108 (C9). http://dx.doi.org/10.1029/2002JC001454.

Kovačević, V., Manca, B.B., Ursella, L., Schroeder, K., Cozzi, S., Burca, M., Mauri, E., Gerin, R., Notarstefano, G., Deponte, D., 2012. Water mass properties and dynamic conditions of the Eastern Mediterranean in June 2007. Prog. Oceanogr. 104, 59–79. http://dx.doi.org/10.1016/j.pocean.2012.05.006.

Krom, M.D., Emeis, K.C., Van Cappellen, P., 2010. Why is the Eastern Mediterranean phosphorus limited? Prog. Oceanogr. 85, 236–244. http://dx.doi.org/10.1016/j.pocean.2010.03.003.

Langdon, C., 2010. Determination of dissolved oxygen in Seawater by Winkler Titration using the Amperometric Technique. version 1: GO–SHIP.ORG.

Lascaratos, A., Williams, R.G., Tragou, E., 1993. A mixed–layer study of the formation of Levantine intermediate water. J. Geophys. Res. 98, 14739. http://dx.doi.org/10.1029/93JC00912.

Lascaratos, A., Roether, W., Nittis, K., Klein, B., 1999. Recent changes in deep water

formation and spreading in the eastern Mediterranean Sea: a review. Prog. Oceanogr. 44, 5–36. http://dx.doi.org/10.1016/S0079-6611(99)00019-1.
Lermusiaux, P.F.J., Robinson, A.R., 2001. Features of dominant mesoscale variability, circulation patterns and dynamics in the strait of sicily. Deep-Sea Res. Part I: Oceanogr. Research Pap. 48, 1953–1997. http://dx.doi.org/10.1016/S0967-0637(00)00114-X.
Lønborg, C., Álvarez-Salgado, X.A., 2014. Tracing dissolved organic matter cycling in the eastern boundary of the temperate North Atlantic using absorption and fluorescence spectroscopy. Deep. Res. Part I 85, 35–46. http://dx.doi.org/10.1016/j.dsr.2013.11.002.
López-Jurado, J.-L., González-Pola, C., Vélez-Belchí, P., 2005. Observation of an abrupt disruption of the longterm warming trend at the Balearic Sea, western Mediterranean Sea, in summer 2005. Geophys. Res. Lett. 32, L24606. http://dx.doi.org/10.1029/2005GL024430.
Luna, G.M., Bianchelli, S., Decembrini, F., De Domenico, E., Danovaro, R., Dell'Anno, A., 2012. The dark portion of the Mediterranean Sea is a bioreactor of organic matter cycling. Global Biogeochem. Cycles, 26, GB2017. http://doi.org/10.1029/2011GB004168.
Malanotte-Rizzoli, P., Artale, V., Borzelli-Eusebi, G.L., Brenner, S., Crise, A., Gacic, M., Kress, N., Marullo, S., Ribera d'AlcalÃ, M., Sofianos, S., Tanhua, T., Theocharis, A., Alvarez, M., Ashkenazy, Y., Bergamasco, A., Cardin, V., Carniel, S., Civitarese, G., D'Ortenzio, F., Font, J., Garcia-Ladona, E., Garcia-Lafuente, J.M., Gogou, A., Gregoire, M., Hainbucher, D., Kontoyannis, H., Kovacevic, V., Kraskapoulou, E., Kroskos, G., Incarbona, A., Mazzocchi, M.G., Orlic, M., Ozsoy, E., Pascual, A., Poulain, P.-M., Roether, W., Rubino, A., Schroeder, K., Siokou-Frangou, J., Souvermezoglou, E., Sprovieri, M., Tintoré, J., Triantafyllou, G., 2014. Physical forcing and physical/biochemical variability of the Mediterranean Sea: a review of unresolved issues and directions for future research. Ocean Sci. 10, 281–322. http://dx.doi.org/10.5194/os-10-281-2014.
Maqbool, T., Cho, J., Hur, J., 2017. Spectroscopic descriptors for dynamic changes of soluble microbial products from activated sludge at different biomass growth phases under prolonged starvation. Water Res. 123, 751e760. http://doi.org/10.1016/j.watres.2017.07.033.
Manca, B.B., Budillon, G., Scarazzato, P., Ursella, L., 2003. Evolution of dynamics in the Eastern Mediterranean affecting water mass structures and properties in the Ionian and Adriatic Seas. J. Geophys. Res. 108, 1–19. http://dx.doi.org/10.1029/2002JC001664.
Manzella, G.M.R., La Violette, P.E., 1990. The seasonal variation of water mass content in the western Mediterranean and its relationship with the inflows through the straits of Gibraltar and Sicily. J. Geophys. Res. 95, 1623. http://dx.doi.org/10.1029/JC095iC02p01623.
Martínez-Pérez, A.M., Álvarez-Salgado, X.A., Arístegui, J., Nieto-Cid, M., 2017a. Deep–ocean dissolved organic matter reactivity along the Mediterranean Sea: does size matter? Sci. Rep. 7, 5687. http://dx.doi.org/10.1038/s41598-017-05941-6.
Martínez-Pérez, A.M., Osterholz, H., Nieto-Cid, M., Dittmar, T., Álvarez-Salgado, X.A., 2017b. Molecular composition of dissolved organic matter in the Mediterranean Sea. Limnol. Oceanogr. 62, 2699–2712. http://dx.doi.org/10.1002/lno.10600.
MEDOC group, 1970. Observation of formation of deep water in the Mediterranean Sea, 1969. Nature 227, 1037–1040. http://dx.doi.org/10.1038/2271037a0.
Millot, C., 1999. Circulation in the Western Mediterranean Sea. J. Mar. Syst. 20, 423–442. http://dx.doi.org/10.1016/S0924-7963(98)00078-5.
Millot, C., 2013. Levantine Intermediate Water characteristics: an astounding general misunderstanding!; Las características de LIW: un malentendido asombroso. Scientia Marina 77, 217–232. http://dx.doi.org/10.3989/scimar.04045.30H.
Mladenov, N., Sommaruga, R., Morales-Baquero, R., Laurion, I., Camarero, L., Diéguez, M.C., Camacho, A., Delgado, A., Torres, O., Chen, Z., Felip, M., Reche, I., 2011. Dust inputs and bacteria influence dissolved organic matter in clear alpine lakes. Nat. Comms. 2, 405. http://dx.doi.org/10.1038/ncomms1411.
Mopper, K., Kieber, D.J., 2002. Photochemistry and cycling of carbon, sulfur, nitrogen and phosphorus. In: Hansell, D.A., Carlson, C.A. (Eds.), Biogeochemistry of Marine Dissolved Organic Matter. Academic, San Diego, California, pp. 455–507.
Moutin, T., Raimbault, P., 2002. Primary production, carbon export and nutrients availability in western and eastern Mediterranean Sea in early summer 1996 (MINOS cruise). J. Mar. Syst. 33–34, 273–288. http://dx.doi.org/10.1016/S0924-7963(02)00062-3.
Nelson, N.B., Siegel, D.A., Carlson, C.A., Swan, C.M., Smethie, W.M., Khatiwala, S., 2007. Hydrography of chromophoric dissolved organic matter in the North Atlantic, Deep Sea Res. Part I 54, 710–731. http://dx.doi.org/10.1016/j.dsr.2007.02.006.
Nelson, N.B., Carlson, C.A., Steinberg, D.K., 2004. Production of chromophoric dissolved organic matter by Sargasso Sea microbes. Mar. Chem. 89, 273–287. http://dx.doi.org/10.1016/j.marchem.2004.02.017.
Nelson, N.B., Siegel, D.A., Michaels, A.F., 1998. Seasonal dynamics of colored disolved material in the Sargasso Sea. Deep Sea Res. Part I 45, 931–957.
Nelson, N.B., Siegel, D.A., 2002. Chromophoric DOM in the open ocean. In: Hansell, D.A., Carlson, C.A. (Eds.), Biogeochemistry of Marine Dissolved Organic Matter. Academic, San Diego, California, pp. 547–578.
Nelson, N.B., Siegel, D.A., Carlson, C.A., Swan, C.M., 2010. Tracing global biogeo– chemical cycles and meridional overtuning circulation using chromophoric dissolved organic matter. Geophys. Res. Lett. 37, L03610. http://dx.doi.org/10.1029/2009GL042325.
Organelli, E., Bricaud, A., Antoine, D., Matsuoka, A., 2014. Seasonal dynamics of light absorption by chromophoric dissolved organic matter (CDOM) in the NW Mediterranean Sea (BOUSSOLE site). Deep Sea Res. Part I 91, 72–85. http://dx.doi.org/10.1016/j.dsr.2014.05.003.
Özturgut, E., 1976. The Source and Spreading of the Levantine Intermediate Water in the Eastern Mediterranean. Saclant ASW Research Center Memorandum Sm–92. La Spezia, Italy 45.
Pérez, F.F., Mouriño, C., Fraga, F., Ríos, A.F., 1993. Displacement of water masses and remineralization rates off the Iberian Peninsula by nutrient anomalies. J. Mar. Res. 51, 1–24. http://dx.doi.org/10.1357/0022240933223891.
Pérez, G.L., Galí, M., Royer, S.J., Sarmento, H., Gasol, J.M., Marrasé, C., Simó, R., 2016. Bio–optical characterization of offshore NW Mediterranean waters: CDOM contribution to the absorption budget and diffuse attenuation of downwelling irradiance. Deep-Sea Res. Part I 114, 111–127. http://dx.doi.org/10.1016/j.dsr.2016.05.011.
Pitta, E., Zeri, C., Tzortziou, M., Mousdis, G., Scoullos, M., 2016. Seasonal variations in dissolved organic matter composition using absorbance and fluorescence spectroscopy in the Dardanelles Straits – North Aegean Sea mixing zone. Cont. Shelf Res. 149, 82–95. http://dx.doi.org/10.1016/j.csr.2016.07.013i.
Poole, R., Tomczak, M., 1999. Optimum multiparameter analysis of the water mass structure in the Atlantic Ocean thermocline. Deep Sea Res. Part I 46, 1895–1921. http://dx.doi.org/10.1016/50967-0637(99).
Powley, H.R., Dürr, H.H., Lima, A.T., Krom, M.D., Van Cappellen, P., 2016. Direct discharges of domestic wastewater are a major source of phosphorus and nitrogen to the Mediterranean Sea. Environ. Sci. Technol. 50, 8722–8730. http://dx.doi.org/10.1021/acs.est.6b01742.
Puig, P., de Madron, X.D., Salat, J., Schroeder, K., Martín, J., Karageorgis, A.P., Palanques, A., Roullier, F., Lopez-Jurado, J.L., Emelianov, M., Moutin, T., Houpert, L., 2013. Thick bottom nepheloid layers in the western Mediterranean generated by deep dense shelf water cascading. Prog. Oceanogr. 111, 1–23. http://dx.doi.org/10.1016/j.pocean.2012.10.003.
Pujo-Pay, M., Conan, P., 2003. Seasonal variability and export of Dissolved Organic Nitrogen in the NorthWestern Mediterranean Sea. J. Geophys. Res. 108, 1901–1911. http://dx.doi.org/10.1029/2000JC000368.
Pujo-Pay, M., Conan, P., Oriol, L., Cornet-Barthaux, V., Falco, C., Ghiglione, J.-F., Goyet, C., Moutin, T., Prieur, L., 2011. Integrated survey of elemental stoichiometry (C, N, P) from the western to eastern Mediterranean Sea. Biogeosciences 8, 883–899. http://dx.doi.org/10.5194/bg-8-883-2011.
R Development Core Team, 2014. R: A language and environment for statistical computing. In: R Foundation for Statistical Computing, Vienna, Austria. ISBN 3–900051–07–0, http://R-project.org.
Reygondeau, G., Guieu, C., Benedetti, F., Irisson, J.-O., Ayata, S.-D., Gasparini, S., Koubbi, P., 2017. Biogeochemical regions of the Mediterranean Sea: an objective multidimensional and multivariate environmental approach. Prog. Oceanogr. 151, 138–148. http://dx.doi.org/10.1016/j. pocean.2016.11.001.
Roether, W., Manca, B.B., Klein, B., Bregant, D., Georgopoulos, D., Beitzel, V., Kovacevic, V., Luchetta, A., 1996. Recent changes in Eastern Mediterranean Deep Waters. Science 271, 333–335.
Roether, W., Klein, B., Beitzel, V., Manca, B.B., 1998. Property distributions and transient–tracer ages in Levantine Intermediate Water in the Eastern Mediterranean. J. Mar. Syst. 18, 71–87.
Roether, W., Klein, B., Manca, B.B., Theocharis, A., Kioroglou, S., 2007. Transient Eastern Mediterranean deep waters in response to the massive dense–water output of the Aegean Sea in the 1990s. Prog. Oceanogr. 74, 540–571. http://dx.doi.org/10.1016/j.pocean.2007.03.001.
Romera–Castillo, C, Letscher, R.T., Hansell, D.A., 2016. New nutrients exert fundamental control on dissolved organic carbon accumulation in the surface Atlantic Ocean. PNAS 113 (38). http://doi.org/10.1073/pnas.1605344113.
Rubino, A., Hainbucher, D., 2007. A large abrupt change in the abyssal water masses of the eastern Mediterranean. Geophys. Res. Lett. 34, L23607. http://dx.doi.org/10.1029/2007GL031737.
Salat, J., Font, J., 1987. Water mass structure near and offshore the catalan coast during the winters of 1982 and 1983. Ann. Geophy. 5B, 49–54.
Santana-Falcón, Y., Álvarez-Salgado, X.A., Pérez-Hernández, M.D., Hernández-Guerra, A., Mason, E., Arístegui, J., 2017. Organic carbon budget for the eastern boundary of the North Atlantic subtropical gyre: major role of DOC in mesopelagic respiration. Sci. Rep. 7, 10129. http://dx.doi.org/10.1038/s41598-017-10974-y.
Santinelli, C., 2015. DOC in the Mediterranean Sea. In: Hansell, D.A., Carlson, C.A. (Eds.), Biogeochemistry of Marine Dissolved Organic Matter, second ed. Academic Press, Boston, pp. 579–608.
Santinelli, C., Follett, C., Brogi, S.R., Xuc, L., Repeta, D., 2015. Carbon isotope measurements reveal unexpected cycling of disolved organic matter in the deep Mediterranean Sea. Mar. Chem. 177, 267–277. http://dx.doi.org/10.1016/j.marchem.2015.06.018.
Santinelli, C., Hansell, D.A., Ribera d'Alcalà, M., 2013. Influence of stratification on marine dissolved organic carbon (DOC) dynamics: the Mediterranean Sea case. Prog. Oceanogr. 119, 68–77.
Santinelli, C., Ibello, V., Lavezza, R., Civitarese, G., Seritti, A., 2012. New insights into C, N and P stoichiometry in the Mediterranean Sea: the Adriatic Sea case. Cont. Shelf Res. 44, 83–93. http://dx.doi.org/10.1016/j.pocean.2013.06.001.
Santinelli, C., Nannicini, L., Seritti, A., 2010. DOC dynamics in the meso and bathypelagic layers of the Mediterranean Sea. Deep-Sea Res. II 57, 1446–1459. http://dx.doi.org/10.1016/j.dsr2.2010.02.014.
Schlitzer, R., Ocean Data View, http://odv.awi.de, 2017.
Schlitzer, R., Roether, W., Oster, H., Junghansh, H., Hausmann, M., Johannsen, H., Michelato, A., 1991. Chlorofluoromenthane and oxygen in the Eastern Mediterranean. Deep Sea Res. 38, 1531–1551.
Schroeder, K., Gasparini, G.P., Tangherlini, M., Astraldi, M., 2006. Deep and intermediate water in the western Mediterranean under the influence of the eastern Mediterranean Transient. Geophys. Res. Lett. 33 (21), L21607. http://dx.doi.org/10.1029/2006.
Schroeder, K., García-Lafuente, J., Josey, S.A., Artale, V., Nardelli, B.B., et al., 2012. Chapter 3, Circulation of the Mediterranean Sea and its variability, In: The climate of the Mediterranean Region - from the past to the future, Lionello, P. (Ed.), Elsevier,

592pp.
Schroeder, K., Chiggiato, J., Bryden, H.L., Borghini, M., Ismail, S.B., 2016. Abrupt climate shift in the Western Mediterranean Sea. Sci. Rep. 6, 23009. http://dx.doi.org/10.1038/srep23009.
Sempéré, R., Para, J., Tedetti, M., Charrière, B., Mallet, M., 2015. Variability of solar radiation and CDOM in surface coastal waters of the Northwestern Mediterranean Sea. Photochem. Photobiol. 91 (4), 851–861.
Siegel, D.A., Maritorena, S., Nelson, N.B., Hansell, D.A., Lorenzi-Kayser, M., 2002. Global distribution and dynamics of colored dissolved and detrital organic materials. J. Geophys. Res. 107 (C12), 3228. http://dx.doi.org/10.1029/2001JC000965.
Sparnocchia, S., Gasparini, G., Astraldi, M., Borghini, M., Pistek, P., 1999. Dynamics and mixing of the Eastern Mediterranean outflow in the Tyrrhenian basin. J. Mar. Syst. 20, 301–317. http://dx.doi.org/10.1016/S0924-7963(98)00088-8.
Sparnocchia, S., Pietro Gasparini, G., Schroeder, K., Borghini, M., 2011. Oceanographic conditions in the NEMO region during the KM3NeT project (April 2006–May 2009). Nucl. Instrum. Methods Phys. Res., Sect. A 626–627, S87–S90.
Tanhua, T., Hainbucher, D., Schroeder, K., Cardin, V., Álvarez, M., Civitarese, G., 2013. The Mediterranean Sea system: a review and an introduction to the special issue. Ocean Sci. 9, 789–803. http://dx.doi.org/10.5194/os-9-789-2013.
The MerMex Group, 2011. Marine ecosystems' responses to climatic and anthropogenic forcings in the Mediterranean. Prog. Oceanogr. 91 (2), 97–166.
Theocharis, A., Georgopoulos, D., Lascaratos, A., Nittis, K., 1993. Water masses and circulation in the central region of the Eastern Mediterranean: Eastern Ionian, South Aegean and Northwest Levantine, 1986–1987. Deep-Sea Res. Part II 40, 1121–1142. http://dx.doi.org/10.1016/0967-0645(93)90064-T.
Theocharis, A., Nittis, K., Kontoyiannis, H., Papageorgiou, E., Balopoulos, E., 1999. Climatic changes in the Aegean Sea influence the eastern Mediterranean thermohaline circulation (1986–1997). Geophys. Res. Lett. 26, 1617–1620. http://dx.doi.org/10.1029/1999GL900320.
Thingstad, T.F., Hagström, Å., Rassoulzadegan, F., 1997. Accumulation of degradable DOC in surface waters: is it caused by a malfunctioning microbial loop? Limnol. Oceanogr. 42 (2), 398–404.
Tomczak, M., 1999. Some historical, theoretical and applied aspects of quantitative water mass analysis. J. Mar. Res. 57, 275–303. http://dx.doi.org/10.1357/002224099321618227.
UNESCO, 1985. The International System of Units (SI) in oceanography. UNESCO Tech. Pap. Mar. Sci. 45, 1–124.
UNESCO, 1986. Progress on oceanographic tables and standards 1983–1986. Work and recommendations of UNESCO/SCOR/ICES/IAPSO joint panel UNESCO. Tech. Pap. Mar. Sci. 50, 1–59.
Velaoras, D., Krokos, G., Nittis, K., Theocharis, A., 2014. Dense intermediate water outflow from the Cretan Sea: a salinity driven, recurrent phenomenon, connected to thermohaline circulation changes. J. Geophys. Res. Oceans 119, 4797–4820. http://dx.doi.org/10.1002/2014JC009937.
Vilibić, I., Orlić, M., 2002. Adriatic water masses, their rates of formation and transport through the Otranto Strait. Deep Sea Res. Part I 49, 1321–1340. http://dx.doi.org/10.1016/S0967-0637(02)00028-6.
Wood, S., 2006. Generalized Additive Models: An Introduction with R. Chapman & Hall, London.
Wu, P., Haines, K., Pinardi, N., 2000. Toward an understanding of deep–water renewal in the Eastern Mediterranean. J. Phys. Oceanogr. 30, 443–458. http://dx.doi.org/10.1175/1520-0485(2000) 030<0443:TAUODW>2.0.CO;2.
Wüst, G., 1961. On the vertical circulation of the Mediterranean Sea. J. Geophys. Res. 66, 3261.
Xing, X., Morel, A., Claustre, H., D'Ortenzio, F., Poteau, A., 2012. Combined processing and mutual interpretation of radiometry and fluorometry from autonomous profiling Bio-Argo floats: 2. Colored Dissolved Organic Matter absorption retrieval. J. Geophys. Res. 117, C04022. http://dx.doi.org/10.1029/2010JC006899.
Xing, X., Claustre, H., Wang, H., Poteau, A., D'Ortenzio, F., 2014. Seasonal dynamics in colored dissolved organic matter in the Mediterranean Sea: patterns and drivers. Deep Sea Res. Part I 83, 93–101. http://dx.doi.org/10.1016/j.dsr.2013.09. 008.
Yacobi, Y.Z., Zohary, T., Kress, N., Hecht, A., Robarts, R.D., Waiser, M., Wood, A.M., Li e, W.K.W., 1995. Chlorophyll distribution throughout the southeastern Mediterranean in relation to the physical structure of the water mass. J. Mar. Sys. 6, 179–190. http://doi.org/10.1016/0924-7963(94)00028-A.